Cell

Ring-shaped odor coding in the antennal lobe of migratory locusts

Graphical abstract

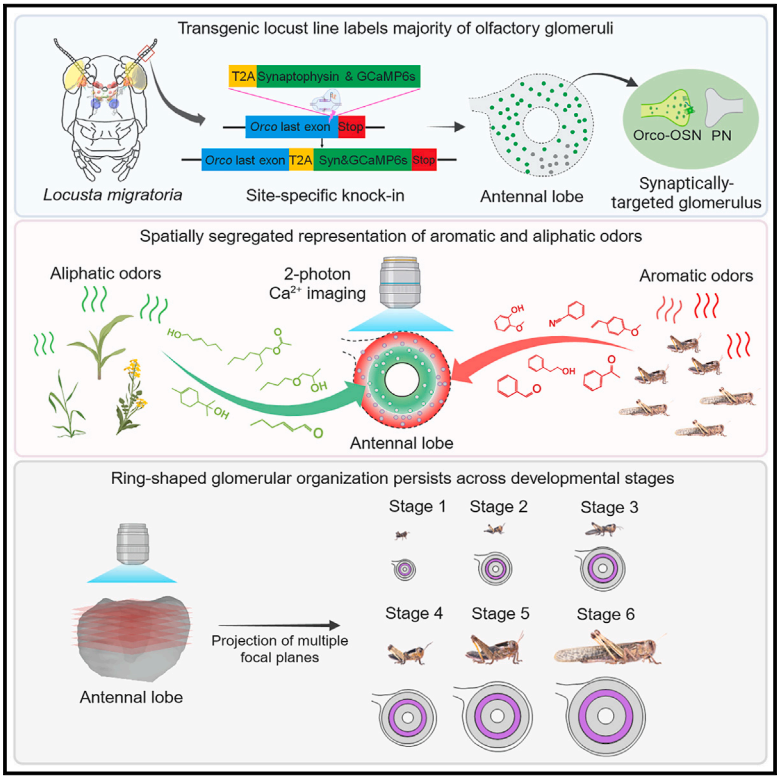

Highlights

- A transgenic line was established to express GCaMP6s in olfactory sensory neurons
- Calcium imaging reveals a functionally ring-shaped odor code of glomerular clusters
- Distinct ring regions encode chemical identity and ecological significance
- The ring-shaped odor-coding pattern occurs consistently throughout development

Authors

Xingcong Jiang, Eleftherios Dimitriou, Veit Grabe, ..., Jürgen Rybak, Bill S. Hansson, Silke Sachse

Correspondence

hansson@ice.mpg.de (B.S.H.), ssachse@ice.mpg.de (S.S.)

In brief

Migratory locusts, genetically expressing the calcium sensor GCaMP6s in olfactory sensory neurons, have an unconventional, ring-shaped olfactory code of glomerular clusters in the antennal lobe, a pattern that occurs consistently throughout development.

Jiang et al., 2024, Cell *187*, 1–19
July 25, 2024 © 2024 The Authors. Published by Elsevier Inc.
https://doi.org/10.1016/j.cell.2024.05.036

CellPress

Please cite this article in press as: Jiang et al., Ring-shaped odor coding in the antennal lobe of migratory locusts, Cell (2024), https://doi.org/10.1016/j.cell.2024.05.036

Cell

CellPress
OPEN ACCESS

Article

Ring-shaped odor coding in the antennal lobe of migratory locusts

Xingcong Jiang,[1,2] Eleftherios Dimitriou,[1] Veit Grabe,[3] Ruo Sun,[4] Hetan Chang,[1] Yifu Zhang,[1] Jonathan Gershenzon,[4] Jürgen Rybak,[1] Bill S. Hansson,[1,5,6,*] and Silke Sachse[2,5,*]

[1]Department of Evolutionary Neuroethology, Max Planck Institute for Chemical Ecology, 07745 Jena, Germany
[2]Research Group Olfactory Coding, Max Planck Institute for Chemical Ecology, 07745 Jena, Germany
[3]Microscopic Service Group, Max Planck Institute for Chemical Ecology, 07745 Jena, Germany
[4]Department of Biochemistry, Max Planck Institute for Chemical Ecology, 07745 Jena, Germany
[5]These authors contributed equally
[6]Lead contact
*Correspondence: hansson@ice.mpg.de (B.S.H.), ssachse@ice.mpg.de (S.S.)
https://doi.org/10.1016/j.cell.2024.05.036

SUMMARY

The representation of odors in the locust antennal lobe with its >2,000 glomeruli has long remained a perplexing puzzle. We employed the CRISPR-Cas9 system to generate transgenic locusts expressing the genetically encoded calcium indicator GCaMP in olfactory sensory neurons. Using two-photon functional imaging, we mapped the spatial activation patterns representing a wide range of ecologically relevant odors across all six developmental stages. Our findings reveal a functionally ring-shaped organization of the antennal lobe composed of specific glomerular clusters. This configuration establishes an odor-specific chemotopic representation by encoding different chemical classes and ecologically distinct odors in the form of glomerular rings. The ring-shaped glomerular arrangement, which we confirm by selective targeting of OR70a-expressing sensory neurons, occurs throughout development, and the odor-coding pattern within the glomerular population is consistent across developmental stages. Mechanistically, this unconventional spatial olfactory code reflects the locust-specific and multiplexed glomerular innervation pattern of the antennal lobe.

INTRODUCTION

Insects rely heavily on their ability to detect and categorize a myriad of odors present in their environment. Olfactory sensory neurons (OSNs) express transmembrane olfactory receptors in their dendritic cilia,[1–4] which are housed within hair-like structures called sensilla located on the chemosensory appendages, the antennae, and the maxillary palps. Each OSN typically expresses a single olfactory receptor gene, encoding an odorant receptor (OR) or ionotropic receptor (IR), along with a universal co-receptor called Orco (associated with ORs)[5–7] or one of the IR8a/IR25a/IR76b co-receptors (related to IRs).[8–10] The axons of OSNs project to the antennal lobe, the primary olfactory center in the insect brain, where they form spherical structures called olfactory glomeruli. Despite considerable variation in the size of the olfactory receptor repertoire across insect species,[11–14] there is generally a "one-to-one" relationship between the number of olfactory receptors and glomeruli.[15] OSNs expressing a given OR converge on the same glomerulus. However, the canonical one-to-one relationship is challenged by recent findings in *Drosophila* and mosquito that reveal the co-expression of multiple chemoreceptors in one OSN.[9,16] Glomeruli receiving information about odors with similar chemical properties also tend to cluster in close proximity within the antennal lobe, contributing to the formation of a "chemotopic map."[15,17–21] Given that insects typically have fewer than 100 ORs and glomeruli,[22] the chemotopic organization within the antennal lobe is less complicated compared with its mammalian counterpart, the olfactory bulb,[23–26] which in, e.g., the mouse contains approximately 3,600 glomeruli.[27]

In insects, a relatively small repertoire of ORs and IRs is still able to encode a wide range of food-related odors based on combinatorial coding, with arrays of different types of OSNs activated to different degrees.[18,28–30] By contrast, the coding of ecologically crucial odors, such as pheromones, appears to follow a particular pattern known as a labeled line coding, in which dedicated pheromone-detecting OSNs project to spatially distinct and narrowly tuned glomeruli.[31–34] To date, studies of the insect olfactory system have mainly focused on holometabolous insects, in which a complete metamorphosis leads to a fundamental reorganization of the antennal lobe between the larval and adult stages, both at molecular and cellular levels.[35–37] By contrast, the much less studied hemimetabolous insects show progressive and less drastic changes in both external and internal morphology during their development. It remains an open question whether fundamental changes in odor-coding patterns within the antennal lobe occur across developmental stages.

This is an open access article under the CC BY-NC license (http://creativecommons.org/licenses/by-nc/4.0/).

Please cite this article in press as: Jiang et al., Ring-shaped odor coding in the antennal lobe of migratory locusts, Cell (2024), https://doi.org/10.1016/j.cell.2024.05.036

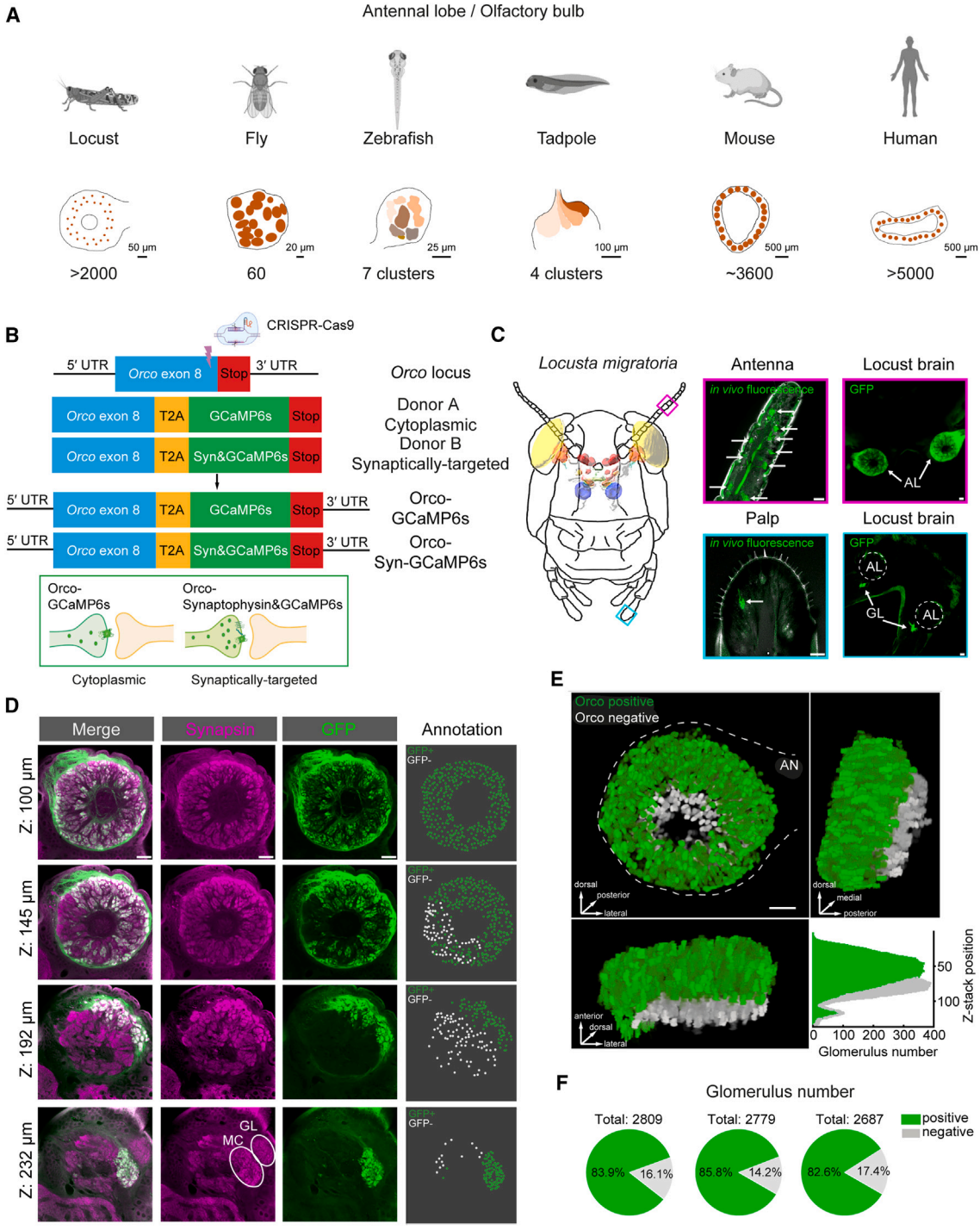

Figure 1. The *Orco-GCaMP6s* transgenic migratory locust reveals glomerular organization in the antennal lobe

(A) Different species display different glomerular organization in their primary olfactory centers. Glomeruli, or clusters of glomeruli, are presented in a laminar view within the insect antennal lobe (locusts and flies) and the vertebrate olfactory bulb (zebrafish, tadpoles, mice, and humans) with the estimated number shown below.[9,22,27,72–74]

(B) Strategy of generating a transgenic locust via CRISPR-Cas9. Two independent transgenic lines were established encoding *Orco-GCaMP6s* (cytoplasmic) and *Orco-Synaptophysin-GCaMP6s* (synaptically targeted), respectively.

(C) *In vivo* GFP fluorescence and immunostaining in the chemosensory organs and the brain. Left, schematic of a locust brain (adapted from the desert locust, *Schistocerca gregaria*: Insect Brain Database, https://insectbraindb.org/app/ [75]) and the main olfactory organs, antenna (magenta) and palp (cyan). Middle,

(legend continued on next page)

Please cite this article in press as: Jiang et al., Ring-shaped odor coding in the antennal lobe of migratory locusts, Cell (2024), https://doi.org/10.1016/j.cell.2024.05.036

The migratory locust (*Locusta migratoria*) and related locust species have gained widespread attention for their swarming behavior, which poses a substantial threat to modern agriculture in large parts of the world. Swarm formation involves transition from a solitary phase to a gregarious phase, and the sensory cues that underlie the subsequent aggregation of tens of thousands of locusts include conspecific odors and pheromones.[38–43] Once swarms are formed, locusts migrate and march toward palatable plants guided by plant-derived cues. The migratory locust genome is large (>6.3 GB) and encodes more than 140 OR genes,[44,45] the majority of which are expressed from nymphal to adult stages.[45] *In vitro* deorphanization of approximately one-third of these OR types revealed extremely narrow tuning characteristics, which distinguishes them from all other insects studied to date.[46] Pathways defined by OR-expressing OSNs are involved in conspecific pheromone-induced attraction, preceding aggregation and swarming.[45] Although the importance of specific pheromone components remains controversial,[39] recent advances have shed light on the detection of the aggregation pheromone 4-vinylanisole (4VA)[42] and the anti-cannibalism pheromone phenylacetonitrile (PAN) in the migratory locust.[47]

Previous studies on hemimetabolous insects, such as crickets and cockroaches, have elucidated the anatomical characteristics and coding properties of general odors and pheromone compounds in the antennal lobe, as well as the spatial receptive fields for odor localization.[48–50] However, locusts, representing a large family of orthopteran species, differ from other hemimetabolous insects in the general organization of the antennal lobe.[22,48,49,51] Over 1,000 glomeruli (in the desert locust)[52] receive input from ten times fewer OSN types.[53] The system thus defies the canonical one-to-one paradigm between OSNs expressing a given individual OR or IR and a corresponding glomerulus: the axon of an individual OSN targets multiple glomeruli in the antennal lobe.[51] Extensive characterization of OSNs and higher-order olfactory neurons in terms of their temporal responses has revealed multiple odor response motifs, synchronization, and plasticity within this intricate olfactory system.[54–58] In addition, central odor processing is plastic across the behavioral transition between the gregarious and solitary phases.[52,59,60] During development, the number of glomeruli increases from several hundred in first instar nymphs to >1,000 in adults.[52] This dynamic transformation suggests that the cellular and molecular substrates underlying olfactory coding may not be uniformly consistent across developmental stages.[52,58]

To gain a deeper understanding of olfactory coding in the non-canonical structure of the locust antennal lobe, capturing odor-induced glomerular population activity is necessary but remains a substantial challenge for most non-model insects.[34,61,62] Fortunately, recent advances in transgenic techniques, particularly the CRISPR-Cas9 system,[63–65] have enabled genetic manipulation also of non-model organisms, including migratory locusts.[42,66]

Here, we established a transgenic line in the migratory locust expressing GCaMP6s in OSNs that innervate a substantial proportion of glomeruli within the antennal lobe and mapped the spatial representation patterns of a diverse array of both monomolecular odors and natural odor mixtures. Our results reveal a chemotopic and functionally ring-shaped glomerular organization in the migratory locust antennal lobe that is represented by distinct glomerular clusters, arising from the locust-specific and multiplexed pattern of glomerular innervation.

RESULTS

The glomerular organization of the locust antennal lobe

The antennal lobe of locusts contains a large number of glomeruli, comparable to those found in the olfactory bulb of mammals and distinguishing the locust from the majority of insects (Figure 1A). A large proportion of OSNs in the locust antenna express Orco.[67] We therefore sought to establish a transgenic line in the migratory locust, *Locusta migratoria*, expressing the Ca^{2+}-sensitive protein GCaMP6s under the control of the endogenous *Orco* promoter, allowing both anatomical and functional characterization of a large proportion of glomeruli within the locust antennal lobe. We employed the CRISPR-Cas9 system to knockin the GCaMP6s coding sequence between the last codon of *Orco* and the stop codon and used a T2A ribosomal skipping sequence such that both Orco and the calcium sensor are expressed as independent proteins (Figure 1B). In addition, to optimize the fluorescence at the axon terminals and to improve the signal-to-noise ratio of Ca^{2+} signals in the antennal lobe, we linked GCaMP6s to synaptophysin, a presynapse-enriched protein (Figure 1B).[68] Thus, the two knockin lines, *Orco-GCaMP6s* and *Orco-Syn-GCaMP6s*, were generated (Figure S1A), of which the latter transgenic line was predominantly used throughout our study. We found that GCaMP6s aggregate at the axonal termini of OSNs in the *Orco-Syn-GCaMP6s* line (Figure S1B), leading to significantly higher fluorescence as compared with the *Orco-GCaMP6s* transgenic line (Figure S1C). Based on the *Orco-Syn-GCaMP6s* line, examination of the raw fluorescence clearly revealed labeled cell clusters in the antenna and palps of gregarious adult females (Figure 1C), where Orco-expressing OSNs are expected to reside.[67,69] Immunostaining of GFP in the locust brain revealed distinguishable central projections from antennae and palps to the antennal lobe and the globular lobe, respectively. The Orco-positive projections from the two chemosensory organs are topographically segregated

in vivo GCaMP6s fluorescence visualized in longitudinally sectioned sensory organs in the *Orco-Synaptohysin-GCaMP6s* transgenic line. Right, GFP immunostaining reveals central projections of peripheral OSNs. AL, antennal lobe; GL, globular lobe. Scale bars, 50 μm.

(D) Glomerular annotation in the migratory locust antennal lobe of the *Orco-Synaptohysin-GCaMP6s* transgenic line. Left three panels, immunostaining of GFP and synapsin. Right, annotation of Orco-positive and Orco-negative glomeruli. MC, median crescent. Scale bars, 50 μm.

(E) Visualization of a 3D reconstructed migratory locust antennal lobe. Upper left, dorsal view; upper right, medial view; lower left, lateral view. AN, antenna nerve. Lower right, count of glomeruli for each focal plane. Scale bars, 50 μm.

(F) Percentage of Orco-positive and Orco-negative glomeruli out of the complete glomerular array in three samples.

See also Figure S1.

Please cite this article in press as: Jiang et al., Ring-shaped odor coding in the antennal lobe of migratory locusts, Cell (2024), https://doi.org/10.1016/j.cell.2024.05.036

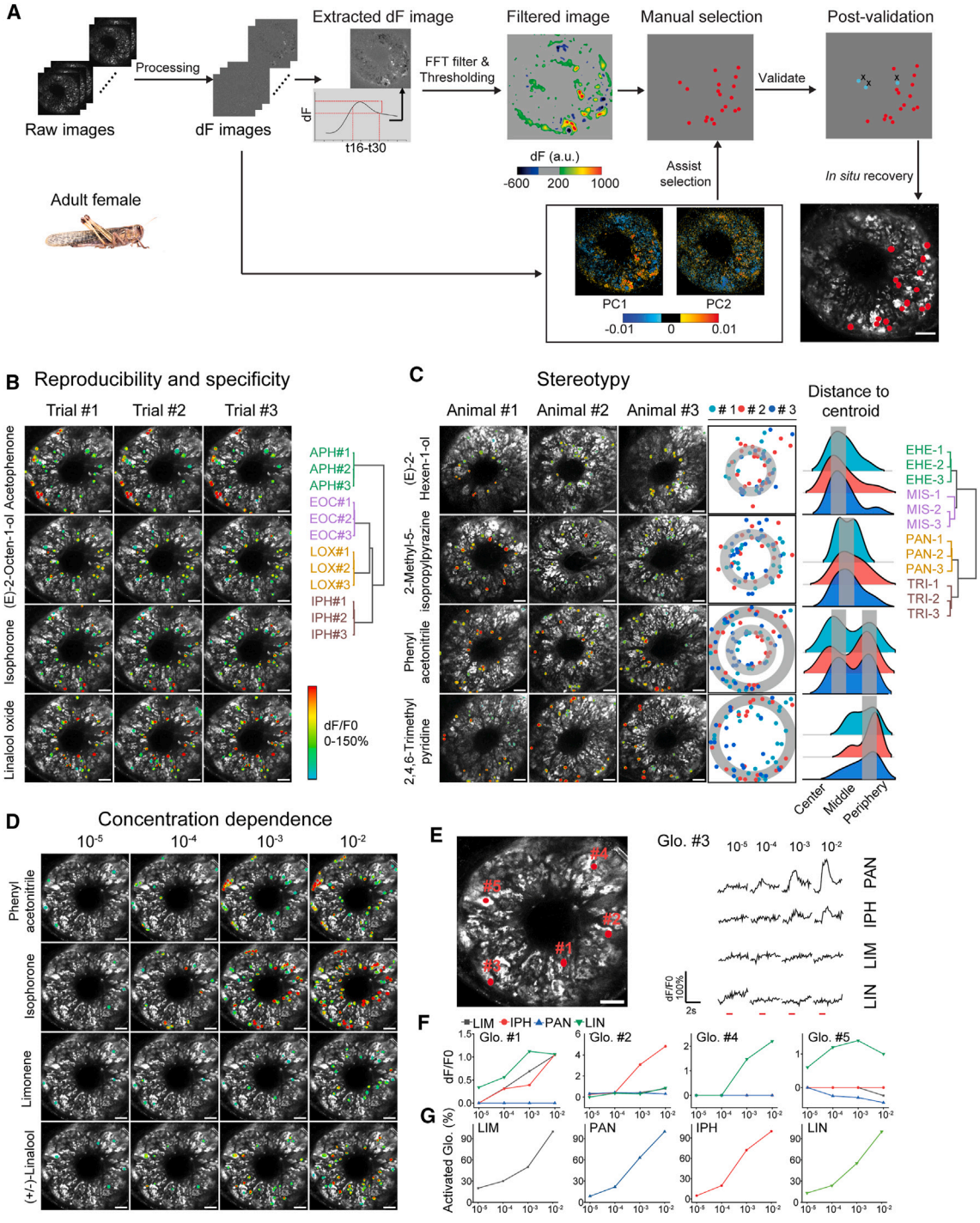

Figure 2. Odor-induced robust, stereotypic, and specific glomerular responses in the migratory locust antennal lobe

(A) Workflow of two-photon imaging data processing and extraction of activated glomeruli. Procedure to select and validate responsive regions of interest (ROIs) is exemplified by the response with phenylacetonitrile (PAN, 10^{-3}, v/v) in a gregarious female adult. For simplicity, only identification, and validation of excited ROIs are represented. For further details, see STAR Methods.

(B) Odor-induced response patterns across three trials are highly reproducible. Left three panels, odor map of extracted responsive glomeruli in the antennal lobe of an adult female after stimulation with four odors (concentration: 10^{-3}) obtained with two-photon microscopy. Cosine distances were calculated in a hierarchical clustering analysis using the 12 response maps.

(C) Representative odor-induced and stereotypic response patterns in three individuals. Left three panels, odor map of extracted responsive glomeruli after stimulation with four odors (10^{-3}). 4th panel, overlay of responsive glomeruli from three adult females. The response intensity for each glomerulus was not taken

(legend continued on next page)

Please cite this article in press as: Jiang et al., Ring-shaped odor coding in the antennal lobe of migratory locusts, Cell (2024), https://doi.org/10.1016/j.cell.2024.05.036

(Figure 1C). To confirm selective central brain labeling from OSNs, one antenna was removed, and the GFP labeling was examined after 10 days. As expected, this unilateral antenna ablation abolished the GFP immunofluorescence in the antennal lobe on the ablated side, indicating exclusive labeling from ipsilateral antennal OSNs as well as the absence of bilateral OSN innervation in the locust antennal lobe (Figure S1D). By double-immunostaining of GFP and synapsin, we manually segmented and 3D reconstructed individual glomeruli in the antennal lobe of gregarious adult females using the *Orco-Syn-GCaMP6s* line (Figure 1D). We found that the anterior region of the antennal lobe exclusively contains Orco-positive glomeruli and that Orco-negative glomeruli begin to appear in a near-medial layer. In the posterior region, the median crescent, a neuropil consisting of compact glomeruli, receives only Orco-positive input (Figure 1D; Video S1). Notably, the diameter of single glomeruli varies considerably when observed through a single focal plane, with the majority within a range of 10–20 μm (Figure S1E). 3D-visualization of the reconstructed antennal lobe revealed a clear topographic separation between Orco-positive and Orco-negative glomeruli (Figure 1E; Video S2). Glomeruli numbered 2,687–2,809 among the three reconstructed specimens of gregarious adult females, and >80% of glomeruli were Orco-positive in all three females (Figure 1F), indicating that the gross glomerular organization is conserved across individuals (Figures S1F and S1G). In comparison, mosquitoes and vinegar flies have approximately 50% (33/68) and 75% (45/60) Orco-positive glomeruli, respectively.[9,70] This proportional expansion suggests an enhanced role for Orco-dependent chemosensation compared with its counterparts, the IRs. Recent studies in mosquitoes and vinegar flies have revealed a cooperative olfactory functional mode involving both OR and IR pathways within the same OSN.[16] In locusts, such evidence of co-localization between the two types of co-receptors is so far lacking, at least at the mRNA level.[71] Taken together, we have established transgenic lines for the migratory locust that drive GCaMP6s expression from the endogenous *Orco* promoter and genetically label the majority of OSNs and glomeruli in the antennal lobe.

The locust antennal lobe reveals a ring-shaped chemotopic organization

To examine the odor-coding properties of Orco-expressing OSNs in our transgenic line, we characterized odor-induced Ca^{2+} responses using a two-photon microscope. Application of odors evoked dynamic fluorescence changes in specific antennal lobe regions of gregarious adult females. Based on the temporal response properties, we established a stringent semi-automated workflow that allowed the extraction of odor-responsive glomeruli (Figure 2A). We first quantified the general odor-coding properties at the level of a single focal plane before performing systematic measurements over multiple planes. To determine whether odor-evoked glomerular responses are reproducible between trials, we applied four odors and monitored the Ca^{2+}-signals in three consecutive trials at a single focal plane. Notably, repetitive stimulation with the same odor induced highly similar response patterns across the three trials, with each individual odor activating a specific and partly overlapping subset of glomeruli, which could be clearly separated via a clustering analysis (Figures 2B and S2A). We investigated next whether the odor-evoked response patterns are similar between different animals (Figures 2C and S2B). Superimposing the extracted glomerular responses for each odor reveals that odor-evoked responses are organized in a ring-shaped pattern, concentrically organized around the central hub, which is occupied by the projection neuron (PN) tract and therefore does not contain glomeruli. Notably, the centroid-oriented distribution of responding glomeruli was very similar in all three animals, as confirmed by clustering analysis, suggesting stereotypical odor-evoked activity patterns (Figure 2C). Unfortunately, due to the large number of glomeruli, it was not possible to identify and assign the odor responses to individual glomeruli. Next, we investigated dose-dependent responses by testing odor concentrations ranging from 10^{-5} to 10^{-2} (v/v). As expected, the response strength generally increased with rising odor concentration, leading to broad response patterns at the highest odor concentration (Figures 2D and S2C). To gain more insight into the response specificity of individual glomeruli, we extracted the response profiles of five glomeruli for different odors (Figure 2E). We found that, e.g., glomerulus #3 was sensitive to PAN and isophorone, even at concentrations as low as 10^{-4} and 10^{-3}, respectively, but did not show any responses to the other two odors, limonene and (+/−)-linalool, even at higher concentrations (Figure 2E). Similarly, the other four glomeruli also exhibited an odor-specific responsiveness and were only tuned to certain odors (Figure 2F). Lower concentrations, such as 10^{-5} and 10^{-4}, evoked low activations and sparse glomerular responses (Figure 2G).

Anatomically identifying and functionally characterizing each glomerulus within the densely packed glomerular organization in the locust antennal lobe proved highly challenging. However, our data indicated that the spatial organization of responsive glomeruli assumed a ring-shaped structure within the locust antennal lobe (Figure 2), suggesting that glomerular responsiveness could be quantified within annuli of a ring-shaped

into account. The gray-shaded ring-shaped glomerular subpopulation corresponds to the peak region (~20% of antennal lobe width), where responsive glomeruli show similar distances to the centroid across three animals (right, #1, #2, and #3). Cosine distances were calculated by hierarchical clustering analysis using the distribution profile of responsive glomeruli from the 12 response maps.

(D) Increasing odor concentrations induced stronger calcium responses in the antennal lobe. Responsive glomeruli were extracted after stimulation with four odors at increasing concentrations.

(E) Specificity of odor-induced glomerular responses. Left, scanning of a focal plane with five ROIs (red). Right, dynamic traces (dF/F0) of glomerulus #3 in response to four odors. Red lines below indicate the odor stimulation.

(F) Peak responses (dF/F0) induced after stimulation with four odors at different concentrations for glomeruli #1, #2, #4, and #5.

(G) Fraction of activated glomeruli after stimulation at different concentrations relative to the number activated at the highest concentration (10^{-2}).

Scale bars, 50 μm. Data based on female adults. Odor abbreviations are given in the STAR Methods section.

See also Figure S2.

Please cite this article in press as: Jiang et al., Ring-shaped odor coding in the antennal lobe of migratory locusts, Cell (2024), https://doi.org/10.1016/j.cell.2024.05.036

arrangement. To simplify the 3D representation of responsive subpopulations of glomeruli, a single focal plane within the antennal lobe was divided into 16 concentric ring regions based on the relative distance to the centroid (step 2, Figure 3A). The width of each region (~10 μm) generally corresponds to the minimum diameter of a glomerulus at adult stage (Figure S1E). For a given concentric ring region, we calculated the "regional response weight," which integrates the averaged response strength and the population size relative to the total responsive glomerular population in the antennal lobe (steps 3 and 4, Figure 3A). As an example, we quantified a stack of 10 focal planes stimulated by PAN (10^{-3}) in animal #1 (Figure S2D), resulting in a projected odor map of glomerular responses for this animal (Figure S2E). To further elucidate the distribution of the responsive glomeruli across the 16 ring regions, we plotted the position of individual glomeruli in the respective ring regions against their response strength (Figure S2F). We found that PAN elicited a strong activation in both the central and the peripheral antennal lobe regions. Furthermore, the stereotypical odor representation across animals is confirmed by the response weights calculated from multiple focal planes across the 16 regions (Figures S2G and S2H).

In order to generate a comprehensive database of odor-evoked activity patterns in the locust antennal lobe, we selected a total of 46 odors accounting for diverse chemical classes that have been recently identified as specific ligands for locust ORs.[46] Using the above-established methodologies, we acquired the projected response maps for each odor (Figure S3A) and the centroid-oriented distribution of glomerular responses (Figure S3B). We pooled the responses of the glomerular populations over three animals to reduce individual variations (Figure S3C). To analyze the correlations between different odors based on their regional response weights, we performed a clustering analysis. This analysis clearly separated the response patterns into three clusters, each of which included a specific subset of chemical classes (Figure 3B). Clusters 1, 2, and 3 represent those odors that primarily activate the central, central-medial, and peripheral concentric ring regions, respectively (Figure 3B). Next, we asked whether the response-based clustering reflected different chemical structures. To do so, we extracted a set of chemical descriptors for each odor and correlated the chemical descriptors with the regional response weights for each odor-pair (in total, 1,035 pairs). We found a significant but moderate correlation ($r = 0.4$, $p < 10^{-39}$, Figure 3C), indicating that, in general, the chemical structure of an odor determines the odor-evoked response patterns. This correlation is more obvious between clusters 1 and 3 ($r = 0.43$, $p < 10^{-12}$) as well as clusters 2 and 3 ($r = 0.5$, $p < 10^{-14}$), while there is no correlation for clusters 1 and 2 ($r = 0.05$, $p = 0.37$, Figure 3C). Indeed, clusters 1 and 2 comprise a wider range of partly overlapping chemical classes, while cluster 3 consists mainly of simple aromatic and aromatic-like compounds (Figure 3D), the typical volatiles emitted by the migratory locust.[46]

To further illustrate that chemical structure determines the spatial activity pattern of an odor, we constructed the "locust chemospace" by extracting the chemical descriptors for >200 ecologically relevant odors[46] and then performed a dimensionality reduction using a t-distributed stochastic neighbor embedding algorithm (Figure 3E). In this space, the uniqueness of cluster 3 was highlighted by a striking separation of cluster 3 from clusters 1 and 2 (Figure 3E). Moreover, odors within each of the three clusters exhibited different hedonic odor valences (Figure 3D),[46] suggesting that the spatial code of odor representations does not necessarily represent a valence code as shown for other insects.[76]

In addition to excitation, we also found widespread odor-induced inhibitory responses (Figures S4A and S4B). We asked whether the spatial distribution of odor-evoked inhibitions is organized in a similar manner as excitatory odor responses. We therefore examined the spatial patterns of inhibited glomeruli for all tested odors. In contrast to excitation, the distribution of inhibited glomeruli does not segregate into distinct clusters (Figure S4C), which is further illustrated by the distribution of six representative odors that lack clear odor-specific patterns (Figure S4D). Furthermore, the distribution of inhibited glomeruli does not correlate with the chemical structures of the odors tested ($r = 0.07$, Figure S4E). Also, the pairwise correlation of odor-induced spatial representation patterns is more homogeneous for inhibitory responses compared with excitatory responses (Figure S4F). Although odors typically inhibited a substantially lower number of glomeruli compared with excited glomeruli (Figure S4G), the number of odor-induced excited and inhibited glomeruli is highly correlated ($r = 0.59$, $p < 10^{-5}$, Figure S4H), suggesting that a stronger odor-induced excitation is often accompanied by a robust inhibition. Notably, when we examined the topology of all responsive glomeruli, we observed that excitatory responses occurred more frequently in the central region of the antennal lobe, while inhibited glomeruli occupied broader and less structured regions (Figure S4I). Taken together, our results demonstrate that odor-evoked excitatory glomerular responses are organized into distinct concentric ring regions according to chemometric properties.

A spatially segregated code for locust- and plant-derived odor blends

The glomerular responses presented so far were obtained with a large panel of monomolecular odors at a concentration of 10^{-3}. To gain deeper insight into the coding of ecologically relevant odor blends at naturally occurring concentrations, we selected five types of odor sources, including adult locusts (male and female), nymphs (stage 5), two host plants (maize and wheat), and one non-host plant (rapeseed), and monitored glomerular responses to these odors using two-photon imaging (Figure 4A). By focusing on a single focal plane, we found that the locust-derived headspaces selectively elicited stronger responses in the peripheral antennal lobe regions, whereas the headspaces derived from the three plant species mainly activated the central regions (Figure 4B). This distinct and headspace-specific distribution of responsive glomeruli was observed for all five animals tested (Figure 4C), each stimulated with freshly prepared headspaces. Quantifying the regional response weights makes the observed trend even clearer, showing that the plant-derived headspaces induced the highest response weights in the central antennal lobe regions, while the peripheral antennal lobe regions were only weakly activated. By contrast, the locust-derived headspaces induced gradually increasing response weights from the central to the peripheral antennal lobe regions

Please cite this article in press as: Jiang et al., Ring-shaped odor coding in the antennal lobe of migratory locusts, Cell (2024), https://doi.org/10.1016/j.cell.2024.05.036

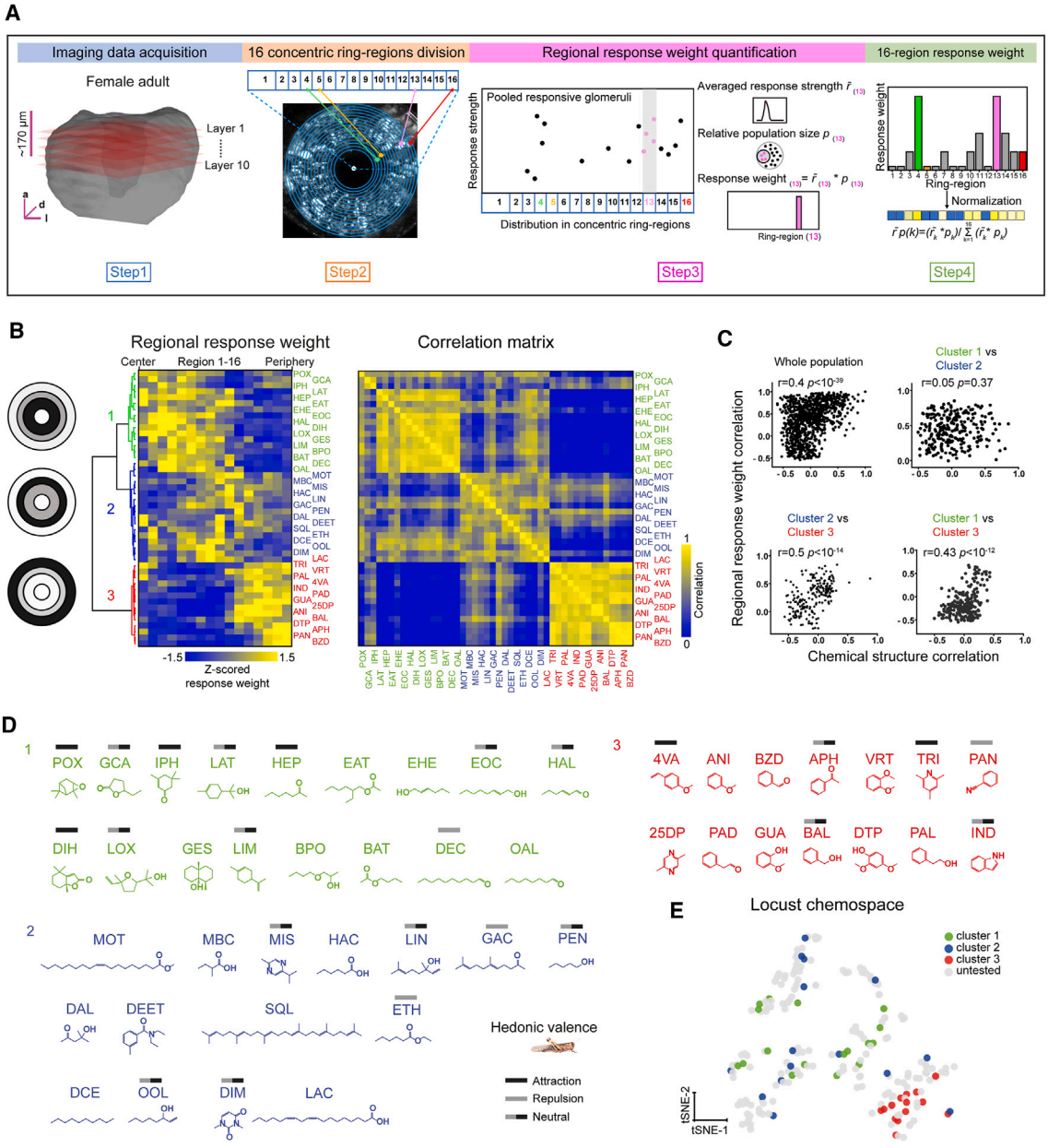

Figure 3. A ring-shaped chemotopic organization in the migratory locust antennal lobe

(A) Workflow for characterizing odor representation profiles within concentric ring-shaped regions in the locust antennal lobe. For details on ring division and response weight calculation, please see STAR Methods.

(B) Hierarchical clustering (left) and Pearson's *r* correlation matrix (right) of regional response weights for 46 odors. Three clusters were identified representing enhanced response weights in the central, central-to-medial, and peripheral glomerular regions.

(C) Pairwise correlation of chemical structures and regional response weights. Data points represent the chemometric similarity and glomerular response similarity in odor pairs over the entire glomerular population (upper left), clusters 1 and 2 (upper right), clusters 2 and 3 (lower left), and clusters 1 and 3 (lower right). r, Pearson's correlation.

(D) Chemical structures of 46 tested odors grouped by the three identified response clusters shown in (E). Hedonic valences of 23 odors investigated in gregarious adult females are marked by gray/black bars.[46]

(E) Embedding the three chemical clusters in the locust chemospace. Tested odors were colored according to their cluster membership in (B); odors comprised in the locust chemospace that were not tested in our study are shown in gray.

Odor name abbreviations are given in the STAR Methods.

See also Figures S2, S3, and S4.

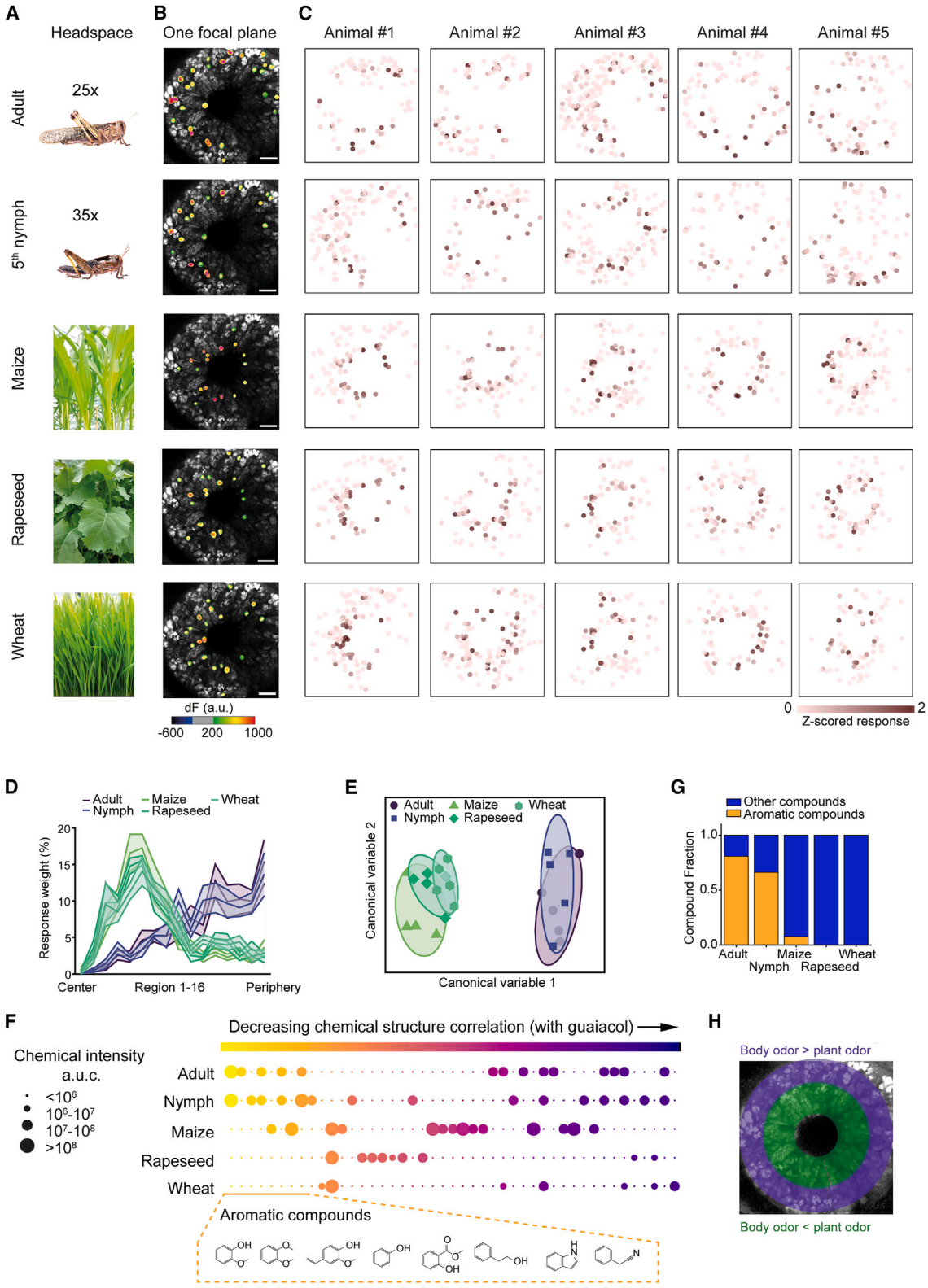

Figure 4. Segregated spatial codes for locust- and plant-produced volatiles in the migratory locust antennal lobe

(A) Five types of headspace derived from locusts (adult and nymphs) and plants (hosts, maize and wheat; non-host, rapeseed).

(B) Response maps elicited by five headspace types in a single focal plane. Only excited glomeruli were extracted. Scale bars, 50 μm.

(legend continued on next page)

Please cite this article in press as: Jiang et al., Ring-shaped odor coding in the antennal lobe of migratory locusts, Cell (2024), https://doi.org/10.1016/j.cell.2024.05.036

(Figure 4D). The distinct response profiles were further illustrated by principal component analysis-discriminant analysis (PCA-DA), which revealed two clearly separated clusters for locust- and plant-derived headspace (Figure 4E).

To explore the underlying basis of these odor-evoked activity patterns, we performed a chemical analysis of the five types of headspace using gas chromatography-mass spectrometry (GC-MS) (Figure 4F). Our analysis revealed that headspaces derived from the adult and nymphal stages were highly similar but notably different from the three plant-derived headspaces (Figure 4G). Importantly, aromatic compounds were highly enriched in the headspaces emitted by locusts but were almost absent from the plant-derived headspaces (Figures 4F and 4G). The contrast observed in both the chemical composition and the spatial representation pattern of the different headspaces is well in line with our previous finding that aromatic compounds predominantly activate the peripheral antennal lobe regions (Figures 3 and 4H).

A consistent pattern of glomerular activations through development

Locusts are hemimetabolous insects and undergo incomplete metamorphosis through five nymphal stages to reach adulthood, resulting in a substantial increase in body size (Figure 5A). In line with this phenomenon, our anatomical quantification revealed substantial changes in the total volume of the locust antennal lobe through development, reminiscent of the gradually increasing number of glomeruli within the antennal lobe of the desert locust.[52] However, the proportion of Orco-positive antennal lobe volume remained stable throughout the six developmental stages (Figure 5B), suggesting a conserved olfactory code in the glomerular population. To test this hypothesis, we first investigated whether the odor-induced ring-shaped glomerular organization also applied to the nymphal stages. We selected a panel of 13 odors representing different chemical classes from the three classified chemical clusters (Figure 3D) and monitored odor-evoked responses at all six developmental stages using two-photon functional imaging (Figure 5C). The response maps as well as the regional response weights were quantified as previously established (Figure 3A). Notably, our data revealed highly correlated response patterns for PAN (10^{-3}) across stages, with stronger responses localized to both the peripheral and central antennal lobe regions, while the odor linalool oxide (10^{-3}) consistently elicited the strongest responses in the central antennal lobe region across all developmental stages (Figure 5D). Furthermore, examination of all 13 odors tested encompassing all replicate animals revealed largely similar regional response weights throughout development (Figure 5E).

Next, we examined the odor responses at the glomerular population level throughout development. We found that stimulation with the 13 selected odors elicited activation of widely distributed glomeruli as imaged in a single focal plane, a feature common to all six stages (Figure 5F). In addition, pairwise correlations of odor responses remained remarkably stable across the six stages (Figure 5G). Overall, the integration of the regional response weight (Figure 5E) and the glomerular population response (Figure 5G) for the 13 odors tested reveals a highly correlated pattern of glomerular activity throughout development, both in terms of the spatial representation and population response (Figure 5H).

Combinatorial coding of distinct chemical identities

Our findings support the existence of a consistent olfactory code through development governed by the entire glomerular population. How are specific glomerular subtypes coordinated to maintain such a "stable" odor code? To identify distinct functional subtypes within the glomerular population, we used our prior dataset encompassing 13 odors tested across six developmental stages, which account for a total of 11,884 responsive glomeruli (Figure 5C). We applied the Louvain clustering algorithm, a method for community detection in large networks. The strength of this clustering algorithm lies in the fact that it allows for a flexible clustering membership by adjusting the resolution, a parameter responsible for the deduced cluster size or number (Figure 6A).[77–79] To determine the possible number of clusters, we adjusted the resolution parameter for five independent analyses using the same dataset. We performed the clustering analyses at resolutions of 1, 0.5, 0.3, 0.2, and 0.1, respectively, resulting in 27, 37, 47, 54, and 71 deduced clusters (Figure S5A). The number 27 corresponds to the default resolution of 1 in the Louvain clustering algorithm. We considered the "animal occurrence rate" to be a critical parameter for the identification of glomerular clusters, as clusters frequently detected in multiple animals are more likely to genuinely exist. We quantified the animal occurrence rate for each adjusted resolution and found that at resolutions from 1 to 0.2, over 90% of the clusters had an animal occurrence rate greater than 80% (Figure S5A). However, at the maximum resolution of 0.1, only 77% of glomerular clusters exhibited a high animal occurrence rate. These results suggest that 0.2 (i.e., 54 glomerular clusters) is the highest resolution at which the majority of the clusters could be identified in >80% of the 39 animals tested (Figure S5B) and were also detected with a high animal occurrence rate for each developmental stage (Figure S5C). This estimate is also in line with a recent study on the functional characterization of ORs in the migratory locust.[46]

To visualize the functional relationships among the 54 identified glomerular clusters, we employed a dimensionality reduction approach using the entire glomerular population (Figure 6A), generating a "glomerular response space" (Figure 6B).

(C) Projected odor maps after stimulation with five headspace types in five animals.
(D) Response weights among the 16 ring-shaped antennal lobe regions for five headspace types. Bold line and shaded area represent mean ± SEM, $n = 5$ animals.
(E) PCA-DA analysis of regional response weights for each headspace. Data points represent individual animals.
(F) GC-MS analysis of five headspace types. Chemical intensity is determined by the area under the chromatogram peak. Odors in the top half of highly enriched chemicals were analyzed by chemical intensity. Structures of locust-produced aromatic compounds are shown below. Chemometric correlation for each compound was compared with guaiacol, the most abundant compound found in locust-derived headspace.
(G) Aromatic compounds are highly enriched in locust-derived headspace but are almost absent from plant volatiles.
(H) Schematic of the segregated spatial representation of locust- and plant-derived volatiles in the antennal lobe.

Please cite this article in press as: Jiang et al., Ring-shaped odor coding in the antennal lobe of migratory locusts, Cell (2024), https://doi.org/10.1016/j.cell.2024.05.036

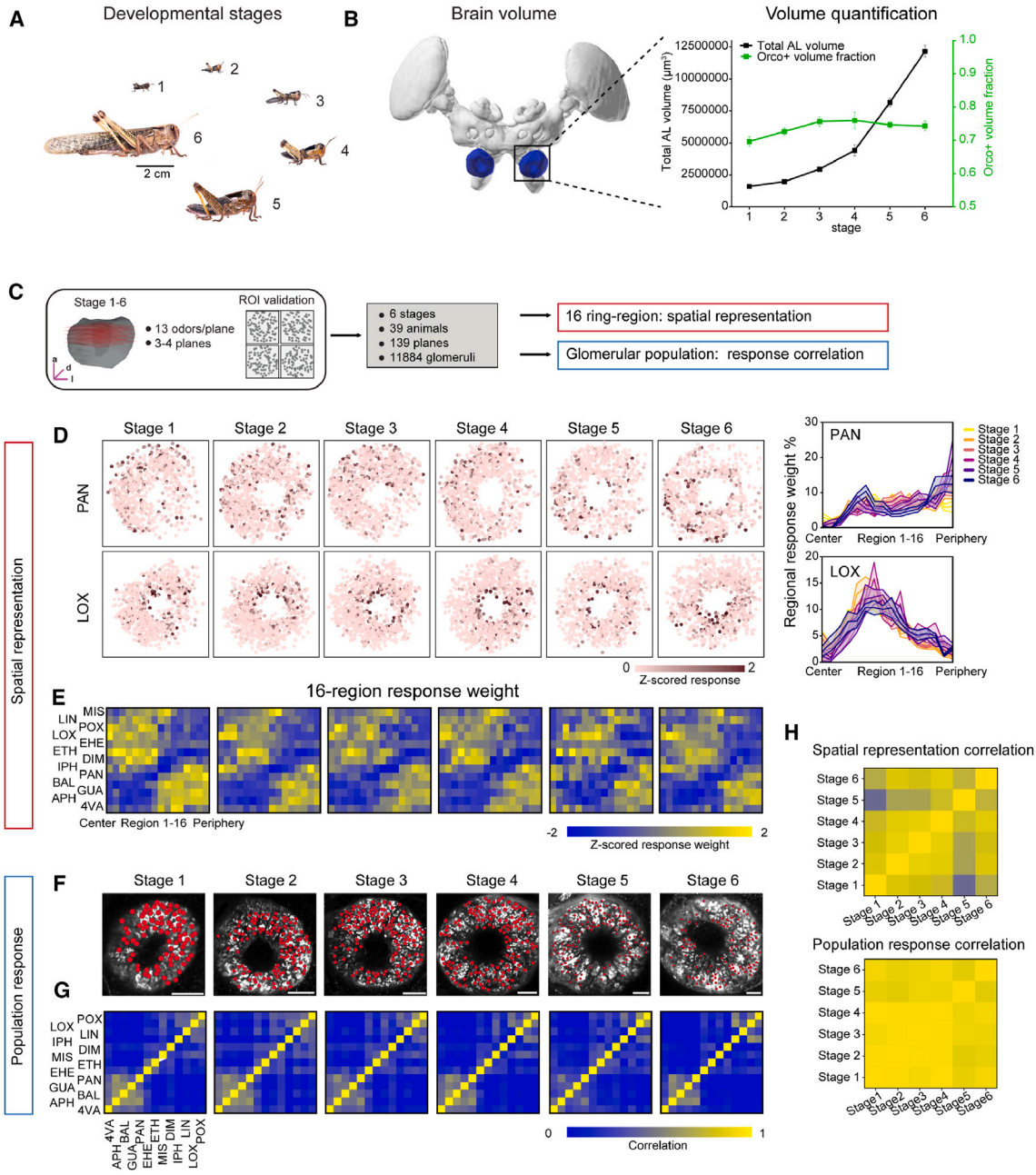

Figure 5. A consistent pattern of odor coding among locust glomeruli throughout development

(A) Body size development of *Locusta migratoria* from nymphal stage 1 to adult stage 6. Scale bars, 2 cm.

(B) Volume development of the entire antennal lobe and the proportion of Orco-positive volume.

(C) Workflow of data acquisition: response patterns to 13 odors were measured for six developmental stages to analyze spatial representation and pairwise odor response correlation.

(D) Projected odor maps after stimulation with PAN and linalool oxide (LOX) across the six developmental stages (n = 22–24 focal planes from 6 to 7 animals per stage). Right, regional response weights for PAN and LOX across six developmental stages. Bold line and shaded area represent mean ± SEM, n = 6–7 animals.

(E) Regional response weights for 13 odors across six developmental stages averaged over 6–7 animals tested.

(F) Spatial distribution of excited glomeruli activated by 13 odors at a single focal plane. Glomeruli displaying an excitatory response to any of the 13 odors were categorized as responsive and marked with a red dot. Scale bars, 50 μm.

(G) Pairwise response correlation for 13 odors across six stages. Glomerular population size: stage 1, 1,641; stage 2, 1,808; stage 3, 2,116; stage 4, 2,119; stage 5, 2,097; stage 6, 2,103.

(H) Correlation quantification of regional response weights and glomerular population response for the 13 odors tested across stages. The data are derived from (E) and (G).

Please cite this article in press as: Jiang et al., Ring-shaped odor coding in the antennal lobe of migratory locusts, Cell (2024), https://doi.org/10.1016/j.cell.2024.05.036

CellPress
OPEN ACCESS

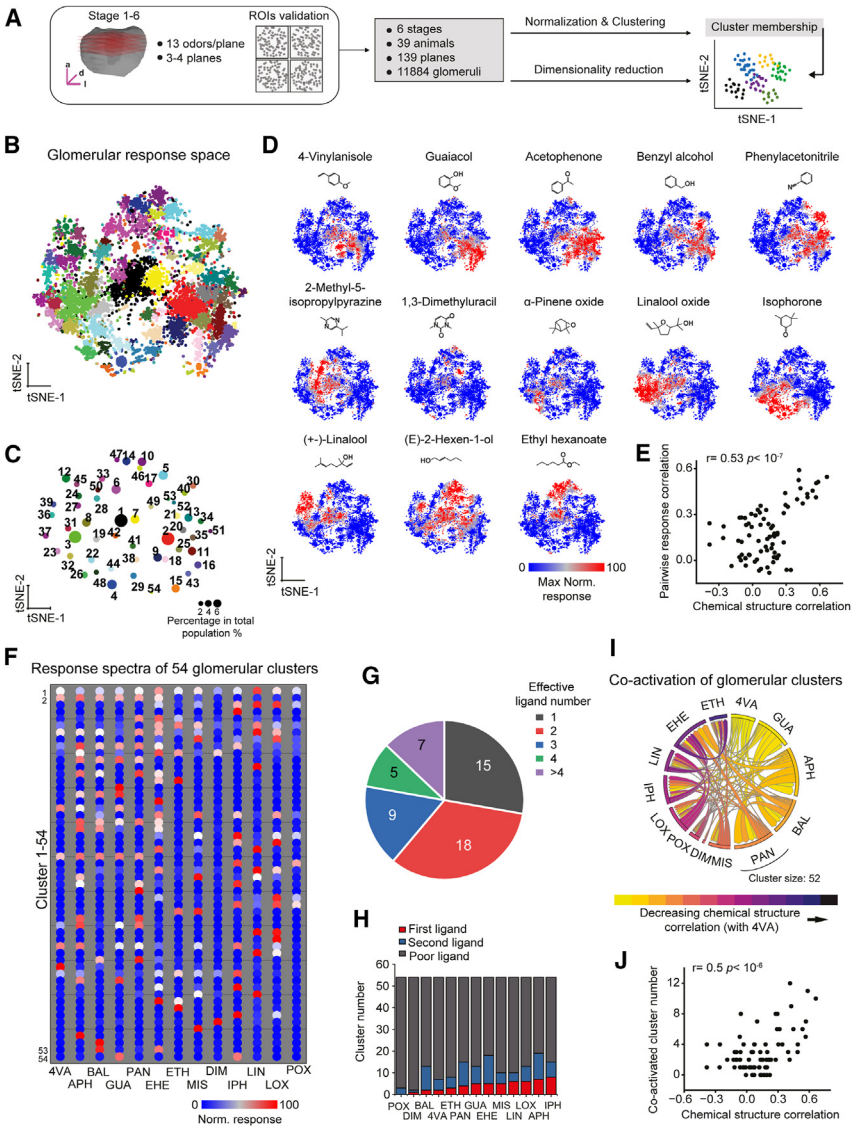

Figure 6. Combinatorial coding of distinct odor identities

(A) Workflow of data acquisition and identification of glomerular clusters.

(B) Location of 54 glomerular clusters in the glomerular response space. For further explanation, see STAR Methods.

(C) Simplified representation of each of the 54 clusters by showing the centroid of the group members, with the dot size proportional to the cluster size.

(D) Odor-specific arrangement patterns in the glomerular response space.

(E) Chemical structure determines glomerular response correlations. r, Pearson correlation.

(F) Response spectra of the 54 glomerular clusters. Data points represent the average of the maximum normalized response of the cluster members included in the coding of a specific odor.

(G) Effective ligand numbers of the 54 clusters. Effective ligands were defined as odors eliciting a response equal to or greater than 50% of the maximum response of a given cluster.

(H) Number of clusters activated by a given odor. First ligand: the best ligand; second ligand: additional effective ligands; poor ligand: odor induced below 50% of the maximum response in a given cluster.

(I) Chord diagram of co-activated glomerular clusters. The size of a link is proportional to the co-activated cluster number. The cluster size for an odor represents the total number of glomerular clusters that are co-activated by that odor and any of the other 12 odors. Odors are displayed clockwise and color coded based on a decrease in chemometric correlation with the odor 4VA.

(J) Odors with similar chemical structures tend to co-activate a larger number of glomerular clusters. *r*, Pearson correlation.

See also Figure S5.

With this virtual space, the membership of each glomerular cluster became discernible (Figures 6B and 6C), and the occupancy of each cluster remained remarkably stable across developmental stages (Figure S5D). Notably, in this virtual space, different chemical identities are represented by distinct subpopulations of glomeruli. These subpopulations vary considerably in size, and their arrangement appears to be determined by the chemometric properties (Figure 6D). This notion was subsequently confirmed by a strong correlation between the chemical structures and the odor-pair relationship encoded by the entire glomerular population (r = 0.53, $p < 10^{-7}$, Figure 6E).

We then examined the response spectra of the 54 glomerular clusters to the 13 odors tested (Figure 6F). We found that more than half of the glomerular clusters responded to only 1–2 effective ligands, while 13% of the clusters were broadly tuned and responded to more than four effective ligands (Figure 6G). There was also a striking heterogeneity in the number of glomerular clusters associated with specific odors: stimulation with acetophenone activated approximately 20 clusters, while only two clusters responded to the odor 1,3-dimethyluracil (Figure 6H). To examine how coding patterns elicited by different chemicals are connected across a fraction of glomerular clusters, we plotted a wiring diagram of co-activated clusters stimulated by specific odor pairs (Figure 6I). This analysis, consistent with a subsequent correlation analysis (r = 0.5, $p < 10^{-6}$), indicates that odors with similar chemical structures are more likely to elicit responses from a larger number of common glomerular clusters, as exemplified by the odor pairs 4VA and acetophenone (chemometric correlation = 0.37, 6 common clusters) and 4VA and ethyl hexanoate (chemometric correlation = 0.04, 2 common clusters, Figure 6J).

We further analyzed the developmental changes regarding cluster size and response strength among the 54 identified glomerular clusters. Although consistently present at each stage, the relative population size of each cluster appeared to be modulated at certain developmental stages when compared

Please cite this article in press as: Jiang et al., Ring-shaped odor coding in the antennal lobe of migratory locusts, Cell (2024), https://doi.org/10.1016/j.cell.2024.05.036

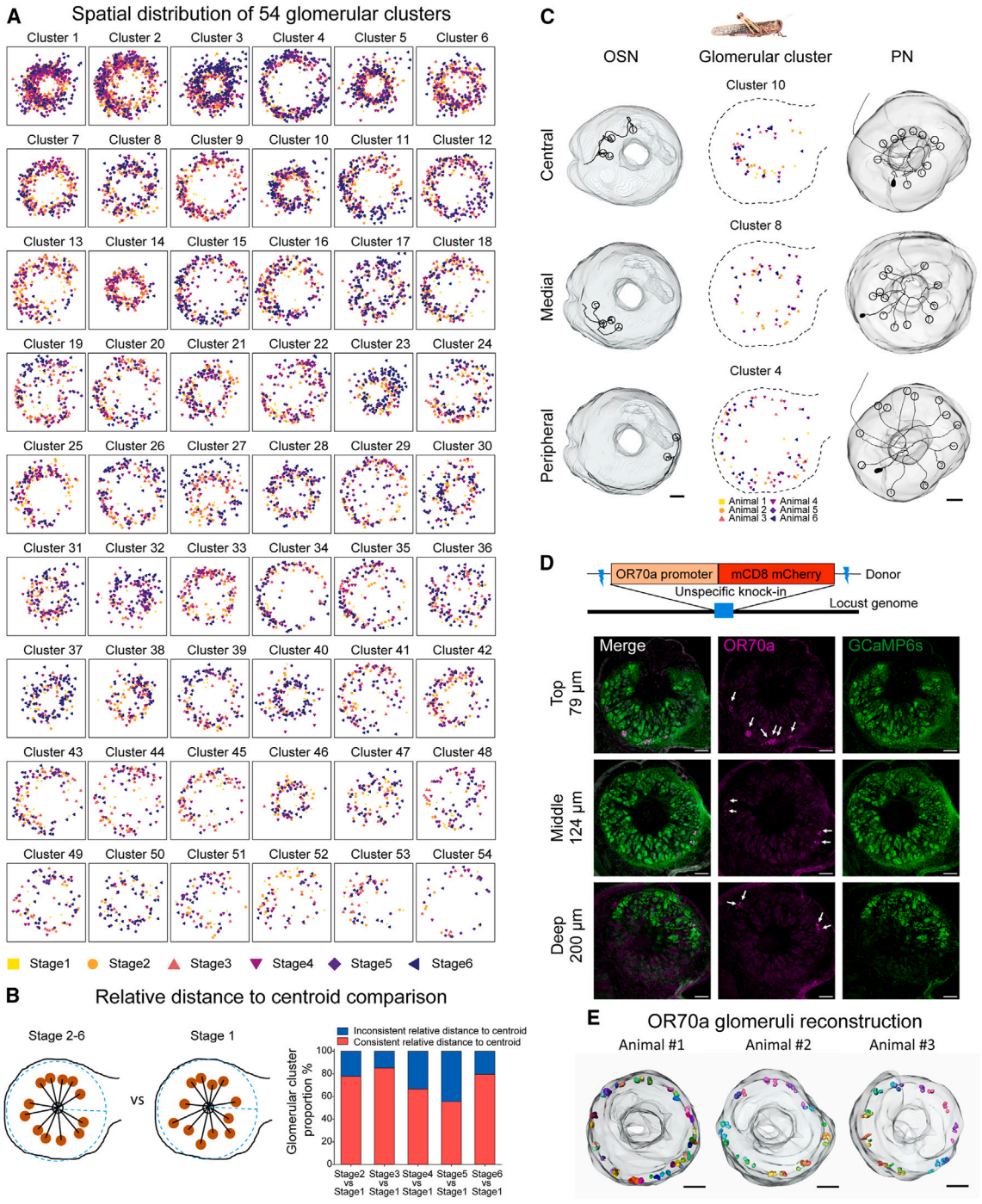

Figure 7. Consistent ring-shaped organization of glomerular clusters through development

(A) Spatial distribution of 54 glomerular clusters in the locust antennal lobe across six developmental stages (n = 22–24 focal planes from 6 to 7 animals per stage).

(B) Comparison of the relative distance to the centroid of the 54 glomerular clusters. Left, relative distance to the centroid was quantified for each member within a particular cluster by comparing distances from stages 2–6 to stage 1. Right, a substantial proportion of clusters maintains a consistent relative distance to the centroid when compared with stage 1. Blue dashed lines indicate boundary and radius of the antennal lobe. For a detailed stage-specific comparison, please see Figure S6B.

(C) Morphological characteristics of OSN axonal innervation, glomerular clusters, and PN dendritic innervation in the locust antennal lobe. Examples of three different glomerular innervation patterns are shown in the central, medial, and peripheral antennal lobe regions. Each innervated glomerulus is marked by a black circle. Data were collected in female adults. Scale bars, 50 μm.

(legend continued on next page)

Please cite this article in press as: Jiang et al., Ring-shaped odor coding in the antennal lobe of migratory locusts, Cell (2024), https://doi.org/10.1016/j.cell.2024.05.036

with its initial state (stage 1, Figure S5E). In addition, a gradual decrease in the general response amplitude was observed as development progressed (Figure S5F). This trend is exemplified by examining the response traces of glomerular clusters to the odor PAN (Figure S5G), as well as the response strength across stages (Figure S5H). The gradual decrease is probably due to a decline in GCaMP6s expression levels in the brain during development as shown by qPCR (Figure S5I). The age-dependent attenuation of the response strength was, however, compensated by data normalization before the subsequent clustering analysis (Figure 6A; see STAR Methods for details). Taken together, the clustering analysis reveals the functional connectivity of specific subpopulations of glomeruli, suggesting that distinct chemical identities are encoded at the level of glomerular clusters in a combinatorial mode.

A ring-shaped organization of glomerular response patterns is maintained across stages

We next asked whether the distribution of the glomerular clusters contributes to the preserved spatial odor patterns across developmental stages. To visualize the spatial distribution of each glomerular cluster, we merged their positions deriving from all examined focal planes onto just one focal plane (Figure 7A). Interestingly, the distribution of all glomerular clusters from six developmental stages shows a consistent ring-shaped structure, with each cluster occupying a distinct concentric ring region. Notably, this ring-shaped structure is not stage-specific and is apparent from the first nymphal stage (Figure S6A). Although we were not able to directly characterize the morphology of individual glomerular clusters, alternatively, we sought to quantify the relative distances to the centroid exhibited by the cluster members (Figure 7B). We found that the majority of glomerular clusters displays consistent (i.e., statistically insignificant) centroid-oriented distances when stages 2–6 were compared with stage 1 as quantified in Figure S6B. This preserved pattern is particularly pronounced when comparing the adult to the first nymphal stage, with over 80% of the glomerular clusters showing this characteristic (Figures 7B and S6B).

We next asked whether the ring-shaped glomerular organization observed in our recorded odor-evoked activities is anatomically substantiated by the innervation patterns of peripheral OSNs as well as central PNs that convey the olfactory information from the antennal lobe to higher brain areas. To explore morphological correlations, we backfilled a large population of individual OSNs and PNs using gregarious female adults and quantified their innervation profiles within the 16 concentric ring regions. We found that all innervated glomeruli of a single OSN or PN fall within a certain antennal lobe region, which aligns well with the distribution patterns of the glomerular clusters (Figures S6C–S6E). Notably, there is a significantly greater number of innervated glomeruli from a single PN compared with an OSN (Figure S6F). The anatomical associations are illustrated by aligning the 3D reconstructions of OSNs and PNs, which show similar glomerular innervation patterns in the central, medial, and peripheral antennal lobe regions, respectively (Figure 7C). Contrary to previous expectations,[80] our neuronal reconstructions revealed that the PN projection patterns in the higher brain centers, such as the mushroom body and lateral horn, do not show a clear differentiation according to their regional innervation patterns observed in the antennal lobe (Figure S6G).

To verify that the ring-shaped glomerular organization is determined by the selective innervation of OSNs expressing a specific OR type, we generated another transgenic locust line that selectively labels the PAN-responsive OR70a (Figure 7D).[47] Immunostaining and 3D reconstruction clearly show that OR70a-OSNs innervate a glomerular population in the peripheral region, spanning the entire antennal lobe along the z axis (Figures 7D and 7E). This distribution pattern is consistent with the activity pattern evoked by PAN (Figures 2 and S2). We also analyzed the potential distribution of other candidate OR types that are functionally correlated with the entire population of 11,884 glomeruli characterized in this study (Figure S7A). To do this, we first embedded the response profiles of individual locust OR types[46] into the glomerular response space and assigned 18 candidate OR types to certain glomerular subpopulations (Figure S7B). Next, we performed clustering analyses with the entire glomerular population and the candidate OR types to reveal their possible spatial distribution in the antennal lobe. In each independent clustering analysis, a candidate OR type was grouped with a subset of the 11,884 glomeruli. Similar to previous operations (Figure S5A), we systematically adjusted the deduced cluster number to highlight a group of ''basic'' glomeruli that occurs in most clustering operations and has therefore a high likelihood to be associated with a particular OR type. For example, based on the clustering results, it is likely that OR6 is associated with a subpopulation of peripheral glomeruli. Remarkably, this predicted spatial distribution pattern remains consistent across all 6 developmental stages (Figure S7C). Likewise, we obtained a likelihood-based distribution map of 18 locust OR types visualized through a merged focal plane (Figure S7D). In the prediction, OR70a is found in both the peripheral and central antennal lobe regions, which is reminiscent of the PAN activity pattern (Figure S2G). This suggests that there may be additional OR types (Figure 6F) that are similarly tuned to OR70a but innervate the central antennal lobe region. By plotting the regional distributions of those glomeruli with high likelihood (i.e., $\geq$0.8), we again found a distinct regional distribution in the locust antennal lobe for each OR type (Figures S7D and S7E). Interestingly, it appears that the three major phylogenetic clades[45] do not necessarily encode a particular distribution pattern in the locust antennal lobe for the encompassed OR types (Figure S7E). In summary,

(D) Immunostaining of OR70a-targeted glomeruli in the transgenic locust line OR70a-mCherry. Upper, expression of mCherry is driven by a clone of *Or70a* promoter. Lower, three representative focal planes show GFP (Orco) and mCherry (OR70a) immunostaining. Glomeruli innervated by OR70a-expressing OSNs are exclusively distributed in the peripheral region of the antennal lobe, marked by white arrows. Scale bars, 50 μm.

(E) 3D reconstruction of glomeruli innervated by OR70a-expressing OSNs. Number of innervated glomeruli: 42 (animal #1), 36 (animal #2), and 39 (animal #3). Different colors indicate individual glomeruli. Data were collected from adult female locusts. Scale bars, 50 μm.

See also Figures S6 and S7.

Please cite this article in press as: Jiang et al., Ring-shaped odor coding in the antennal lobe of migratory locusts, Cell (2024), https://doi.org/10.1016/j.cell.2024.05.036

these results demonstrate that specific glomerular clusters display a consistent and ring-shaped organization that persists throughout all developmental stages.

DISCUSSION

A ring-shaped glomerular organization in the locust antennal lobe

The common blueprint of the olfactory system is based on a high and OR type-specific convergence of OSN axons onto specific glomeruli.[81–83] This formation of molecularly defined glomeruli establishes a spatial and stereotyped odor representation in the antennal lobe and olfactory bulb, which is further reinforced by the predominantly monoglomerular innervation of PNs.[84–86] Although this characteristic glomerular architecture holds true for most species studied to date, other organisms, such as locusts, have evolved a different glomerular architecture.[57,87,88] Here, OSN axons and PN dendrites innervate multiple glomeruli, which, at first glance, appear to lack structural elements. However, our genetic targeting of OSNs expressing the PAN-responsive OR70a reveals that glomeruli receiving the same OSN (i.e., OR type) input are distributed in a highly structured, ring-like manner, resembling an "exploded" glomerulus, culminating in a ring-shaped arrangement of odor-evoked responses within the toroidal locust antennal lobe. Our tracing of individual PNs shows that their dendrites also innervate specific ring regions, thus maintaining the ring-shaped organization at the antennal lobe output level. Hence, insects have evolved different solutions to encode the same features of a sensory stimulus, similar to the existence of salt-and-pepper arrangements and pinwheel arrangements in the visual cortex of rodents and primates, respectively.[89,90]

At this point, it remains largely speculative whether this ring-shaped structure is a less favorable alternative or an improved solution that offers advantages over the glomerular convergence organization. Conceivable advantages would be that the ring-shaped arrangement not only saves space but also prevents the random packing of functionally relevant glomeruli since a ring-like lateral inhibition or excitation would minimize axonal density. Furthermore, within this ring-shaped arrangement, individual glomeruli are functionally connected by multiglomerular PNs with neurites of similar length, potentially facilitating the generation of fast lateral inhibition and synchronized output signals to higher brain centers.[54,91] We also observed a remarkable correlation between the position of the "glomerular ring" and the identity of odors with glomeruli in the peripheral ring regions mainly processing information regarding locust-produced, aromatic compounds, whereas those in the central ring regions receive input from OSNs detecting rather aliphatic plant odors. A segregated code for the detection of conspecifics and plants suggests the presence of two parallel neural pathways, potentially mediating swarming and foraging behaviors in the migratory locust. This phenomenon indicates that spatial olfactory sorting already takes place in the primary olfactory center of the locust brain, providing a more ordered chemotopy than observed in flies and honeybees. Moreover, recent research indicates a lack of chemotopic organization or stereotyped odor representation in the olfactory bulb of the *Xenopus* larva.[92] Its OSNs bifurcate and target multiple glomeruli, similar to locusts, but this lack of organization is mainly attributed to the absence of a fixed and structured glomerular wiring diagram.[92] Thus, the fixed annular pattern of neuronal innervation contributes to stereotypic odor representations in the locust antennal lobe.

Although the presence of a ring-shaped neuronal innervation in the antennal lobe has not been documented in other insects, a similar pattern has been observed in the ellipsoid body of *Drosophila*, a neuropile responsible for spatial orientation, vision, and navigation.[93,94] Here, neurites of R1–R4 neurons localize within distinct ring-shaped regions.[95] However, this neural organization has only been reported in the *Drosophila* ellipsoid body and is absent in the ellipsoid bodies of other insects.[94,96] Thus, these variations in cellular architecture within sensory processing systems illustrate the far-reaching effects of divergent evolution.

Combinatorial odor coding through development

We found that chemical identities are encoded in a combinatorial mode involving specific clusters of glomeruli. By characterizing the odor-coding profiles of 13 chemically diverse odors, we identified 54 glomerular clusters. Although the number of glomerular clusters may be higher after testing more odors, the intrinsic coding logic, such as the combinatorial rule, should remain consistent. The rather broad coding spectra of distinct glomerular clusters are in line with previous findings, where disruption of a single OR responsible for pheromone compounds such as PAN or 4VA did not entirely eliminate neuronal activity or behavioral responses.[42,47] Our finding suggests that these two pheromones are detected by multiple ORs. Notably, the migratory locust genome accommodates a substantial proportion of repetitive sequences[44] and contains scaffolds housing densely arrayed OR genes,[45] indicative of intensified gene duplication and neofunctionalization events, as exemplified by OR34, OR36, and OR39, all tuned to guaiacol.[46] The locust genome may thus have accumulated a certain level of functional redundancy at the level of ORs. Whether this redundancy in molecular elements leads to convergence of glomerular clusters requires further investigation.

The locust olfactory system progressively accumulates cellular and molecular substrates during development but exhibits a surprisingly consistent pattern of glomerular odor coding. This phenomenon is primarily attributed to the occurrence of functionally ring-shaped glomerular clusters across stages, with centroid-oriented distances in the antennal lobe remaining largely consistent throughout development. Unlike what has been found in holometabolous insects, where the glomerular array differs greatly between larva and adult,[18,29,35] the hemimetabolous locust appears to determine the functional repertoire of glomeruli already in the youngest nymphs, and then it remains highly stable through the six developmental stages.[58] Whether or not this is a general characteristic of hemimetabolous insects, however, remains to be investigated.

Beyond a ring-shaped glomerular organization

The chemotopic organization appears to emphasize the coding of chemical structures rather than the hedonic valence of odors.[76] For example, structurally similar pheromones such as

4VA and PAN, of opposite behavioral significance, are both highlighted in the peripheral region, alongside other aromatic compounds displaying neutral hedonic valence. Consequently, the spatial coding representation pattern in the antennal lobe does not provide clear information about odor valence. Also, even though odors evoke different behavioral responses in different stages and phases,[46] their odor code in the antennal lobe appears very similar, and the significance to the individual can thus be expected to be coded in higher brain regions.

In *Drosophila*, single uniglomerular PNs (uPNs) spatially innervate specific regions in higher brain centers, the mushroom bodies, and the lateral horn.[97] Homotypic uPNs, encoding related chemical identities, thus tend to terminate into spatially distinct regions in higher olfactory centers.[98] Interestingly, our results in migratory locusts reveal that, upon receiving input within the ring-shaped glomerular clusters, PNs appear to project their axonal terminals to the higher brain centers in a widespread and uniform pattern, irrespective of the specific innervation patterns in the antennal lobe. This observation raises the possibility that spatial odor-coding patterns in higher brain centers might operate independently of the ring-shaped odor-coding rule found in the antennal lobe. In line with this hypothesis, odors are more sparsely coded in the mushroom body compared with the antennal lobe.[99] In conclusion, we have discovered an unconventional olfactory coding logic in the insect brain, with clusters of glomeruli encoding chemical identities and odor significance in spatially ring-shaped activity patterns. In future studies, it will be interesting to investigate how the ring-shaped logic of odor coding is transformed and integrated in the odor-tuning properties of higher-order neurons.

Limitations of the study

The locust antennal lobe contains a very large number of glomeruli, making it difficult to identify and assign odor responses to individual glomeruli. In addition, its size exceeded the capacity of our two-photon microscope for comprehensive sampling. Future volumetric imaging of the entire antennal lobe will provide further insight into the ring-shaped organization of odor-induced responses, especially in deeper regions. We used a panel of 13 odors to characterize functional glomerular clusters. However, the number of clusters may vary depending on the odors tested, and a larger odor panel would likely reveal more distinct glomerular clusters with similar tuning profiles. Furthermore, a confirmed assignment of specific OR types to the identified glomerular clusters is still lacking and needs to be investigated in future studies.

The ring-shaped glomerular organization, as innervated by OSNs expressing one OR type, has only been demonstrated for OR70a, and we do not know to what extent the expression pattern of the transgenic OR70a line recapitulates the endogenous OR70a expression. Additional transgenic locust lines need to be established to confirm the ring-shaped OSN innervation in the central and middle regions of the antennal lobe. We are thus at the beginning of understanding the intricate coding mechanisms present in the locust antennal lobe. Beyond the experiments suggested above, future transgenic lines allowing functional characterization of the activity in PNs will provide another crucial piece of information.

STAR★METHODS

Detailed methods are provided in the online version of this paper and include the following:

SUPPLEMENTAL INFORMATION

Supplemental information can be found online at https://doi.org/10.1016/j.cell.2024.05.036.

ACKNOWLEDGMENTS

We thank the members of the Department of Evolutionary Neuroethology and the Research Group Olfactory Coding for their helpful advice and discussions, especially Diego Galagovsky for cloning expertise and Nanji Jiang for figure layout. We are grateful to Sabine Brase, Roland Spiess, Chengning Liu, Li, PeiRou Yu, and Lufan Du for assistance with the locust breeding. We also thank the greenhouse team at the Max Planck Institute for Chemical Ecology for providing fresh plants and the workshop for building breeding cages and providing technical support for the two-photon imaging setup. We are grateful to Peter Mombaerts, Max Planck Research Unit for Neurogenetics, for useful comments on the manuscript. We thank Le Kang of the State Key Laboratory of Integrated Management of Pest Insects and Rodents at the Chinese Academy of Sciences (CAS) for providing wild-type migratory locusts. We thank Benjamin Fabian for the locust photos and Martin Nawrot, Michael Schmuker, and Wolfgang Roessler for helpful discussions. This research was supported through funding by the Max Planck Society and the German Science Foundation (DFG) within the priority program SPP2205 (Evolutionary Optimisation of Neuronal Processing).

AUTHOR CONTRIBUTIONS

X.J. designed the transgenic experiments; generated molecular reagents and transgenic lines for *Locusta migratoria*; performed all imaging experiments, chemical headspace acquisition, single OSN staining, and reconstructions; and analyzed all data generated here. X.J. and Y.Z. generated the antennal lobe reconstructions. E.D. and J.R. performed the PN staining and reconstructions. R.S. assisted with the molecular cloning and figure generation and was supervised by J.G. H.C. assisted with the headspace collection and GC-MS analysis. V.G. assisted with the anatomical reconstruction, imaging data acquisition, and data analysis. X.J., B.S.H., and S.S. together conceived the project, designed the experiments, and interpreted the results. X.J., B.S.H., and S.S. wrote the paper, and all authors read, edited, and approved the manuscript for publication. B.S.H. and S.S. supervised the project.

DECLARATION OF INTERESTS

The authors declare no competing interests.

Please cite this article in press as: Jiang et al., Ring-shaped odor coding in the antennal lobe of migratory locusts, Cell (2024), https://doi.org/10.1016/j.cell.2024.05.036

Received: December 1, 2023
Revised: April 5, 2024
Accepted: May 20, 2024
Published: June 18, 2024

REFERENCES

1. Vosshall, L.B., Amrein, H., Morozov, P.S., Rzhetsky, A., and Axel, R. (1999). A spatial map of olfactory receptor expression in the *Drosophila* antenna. Cell *96*, 725–736. https://doi.org/10.1016/S0092-8674(00)80582-6.
2. Clyne, P.J., Warr, C.G., Freeman, M.R., Lessing, D., Kim, J.H., and Carlson, J.R. (1999). A novel family of divergent seven-transmembrane proteins: candidate odorant receptors in *Drosophila*. Neuron *22*, 327–338. https://doi.org/10.1016/S0896-6273(00)81093-4.
3. Smart, R., Kiely, A., Beale, M., Vargas, E., Carraher, C., Kralicek, A.V., Christie, D.L., Chen, C., Newcomb, R.D., and Warr, C.G. (2008). *Drosophila* odorant receptors are novel seven transmembrane domain proteins that can signal independently of heterotrimeric G proteins. Insect Biochem. Mol. Biol. *38*, 770–780. https://doi.org/10.1016/j.ibmb.2008.05.002.
4. Benton, R., Sachse, S., Michnick, S.W., and Vosshall, L.B. (2006). Atypical membrane topology and heteromeric function of *Drosophila* odorant receptors in vivo. PLoS Biol. *4*, e20. https://doi.org/10.1371/journal.pbio.0040020.
5. Vosshall, L.B., Wong, A.M., and Axel, R. (2000). An olfactory sensory map in the fly brain. Cell *102*, 147–159. https://doi.org/10.1016/S0092-8674(00)00021-0.
6. Larsson, M.C., Domingos, A.I., Jones, W.D., Chiappe, M.E., Amrein, H., and Vosshall, L.B. (2004). *Or83b* encodes a broadly expressed odorant receptor essential for *Drosophila* olfaction. Neuron *43*, 703–714. https://doi.org/10.1016/j.neuron.2004.08.019.
7. Neuhaus, E.M., Gisselmann, G., Zhang, W.Y., Dooley, R., Störtkuhl, K., and Hatt, H. (2005). Odorant receptor heterodimerization in the olfactory system of *Drosophila melanogaster*. Nat. Neurosci. *8*, 15–17. https://doi.org/10.1038/nn1371.
8. Benton, R., Vannice, K.S., Gomez-Diaz, C., and Vosshall, L.B. (2009). Variant ionotropic glutamate receptors as chemosensory receptors in *Drosophila*. Cell *136*, 149–162. https://doi.org/10.1016/j.cell.2008.12.001.
9. Task, D., Lin, C.C., Vulpe, A., Afify, A., Ballou, S., Brbic, M., Schlegel, P., Raji, J., Jefferis, G.S.X.E., Li, H.J., et al. (2022). Chemoreceptor co-expression in *Drosophila melanogaster* olfactory neurons. eLife *11*, e72599. https://doi.org/10.7554/eLife.72599.
10. Vulpe, A., and Menuz, K. (2021). *Ir76b* is a co-receptor for amine responses in *drosophila* olfactory neurons. Front. Cell. Neurosci. *15*, 759238. https://doi.org/10.3389/fncel.2021.759238.
11. Missbach, C., Dweck, H.K.M., Vogel, H., Vilcinskas, A., Stensmyr, M.C., Hansson, B.S., and Grosse-Wilde, E. (2014). Evolution of insect olfactory receptors. eLife *3*, e02115. https://doi.org/10.7554/eLife.02115.
12. Karpe, S.D., Jain, R., Brockmann, A., and Sowdhamini, R. (2016). Identification of complete repertoire of *Apis florea* odorant receptors reveals complex orthologous relationships with *Apis mellifera*. Genome Biol. Evol. *8*, 2879–2895. https://doi.org/10.1093/gbe/evw202.
13. McKenzie, S.K., Fetter-Pruneda, I., Ruta, V., and Kronauer, D.J.C. (2016). Transcriptomics and neuroanatomy of the clonal raider ant implicate an expanded clade of odorant receptors in chemical communication. Proc. Natl. Acad. Sci. USA *113*, 14091–14096. https://doi.org/10.1073/pnas.1610800113.
14. Engsontia, P., Sanderson, A.P., Cobb, M., Walden, K.K.O., Robertson, H.M., and Brown, S. (2008). The red flour beetle's large nose: an expanded odorant receptor gene family in *Tribolium castaneum*. Insect Biochem. Mol. Biol. *38*, 387–397. https://doi.org/10.1016/j.ibmb.2007.10.005.
15. Couto, A., Alenius, M., and Dickson, B.J. (2005). Molecular, anatomical, and functional organization of the *Drosophila* olfactory system. Curr. Biol. *15*, 1535–1547. https://doi.org/10.1016/j.cub.2005.07.034.
16. Herre, M., Goldman, O.V., Lu, T.C., Caballero-Vidal, G., Qi, Y.Y., Gilbert, Z.N., Gong, Z.Y., Morita, T., Rahiel, S., Ghaninia, M., et al. (2022). Non-canonical odor coding in the mosquito. Cell *185*, 3104–3123.e28. https://doi.org/10.1016/j.cell.2022.07.024.
17. Bisch-Knaden, S., Dahake, A., Sachse, S., Knaden, M., and Hansson, B.S. (2018). Spatial representation of feeding and oviposition odors in the brain of a hawkmoth. Cell Rep. *22*, 2482–2492. https://doi.org/10.1016/j.celrep.2018.01.082.
18. Hallem, E.A., and Carlson, J.R. (2006). Coding of odors by a receptor repertoire. Cell *125*, 143–160. https://doi.org/10.1016/j.cell.2006.01.050.
19. Wang, J.W., Wong, A.M., Flores, J., Vosshall, L.B., and Axel, R. (2003). Two-photon calcium imaging reveals an odor-evoked map of activity in the fly brain. Cell *112*, 271–282. https://doi.org/10.1016/S0092-8674(03)00004-7.
20. Mertes, M., Carcaud, J., and Sandoz, J.C. (2021). Olfactory coding in the antennal lobe of the bumble bee *Bombus terrestris*. Sci. Rep. *11*, 10947. https://doi.org/10.1038/s41598-021-90400-6.
21. Sachse, S., Rappert, A., and Galizia, C.G. (1999). The spatial representation of chemical structures in the antennal lobe of honeybees: steps towards the olfactory code. Eur. J. Neurosci. *11*, 3970–3982. https://doi.org/10.1046/j.1460-9568.1999.00826.x.
22. Hansson, B.S., and Stensmyr, M.C. (2011). Evolution of insect olfaction. Neuron *72*, 698–711. https://doi.org/10.1016/j.neuron.2011.11.003.
23. Ma, L.M., Qiu, Q., Gradwohl, S., Scott, A., Yu, E.Q., Alexander, R., Wiegraebe, W., and Yu, C.R. (2012). Distributed representation of chemical features and tunotopic organization of glomeruli in the mouse olfactory bulb. Proc. Natl. Acad. Sci. USA *109*, 5481–5486. https://doi.org/10.1073/pnas.1117491109.
24. Johnson, B.A., Xu, Z., Ali, S.S., and Leon, M. (2009). Spatial representations of odorants in olfactory bulbs of rats and mice: similarities and differences in chemotopic organization. J. Comp. Neurol. *514*, 658–673. https://doi.org/10.1002/cne.22046.
25. Wachowiak, M., and Cohen, L.B. (2001). Representation of odorants by receptor neuron input to the mouse olfactory bulb. Neuron *32*, 723–735. https://doi.org/10.1016/S0896-6273(01)00506-2.
26. Burton, S.D., Brown, A., Eiting, T.P., Youngstrom, I.A., Rust, T.C., Schmuker, M., and Wachowiak, M. (2022). Mapping odorant sensitivities reveals a sparse but structured representation of olfactory chemical space by sensory input to the mouse olfactory bulb. eLife *11*, e80470. https://doi.org/10.7554/eLife.80470.
27. Richard, M.B., Taylor, S.R., and Greer, C.A. (2010). Age-induced disruption of selective olfactory bulb synaptic circuits. Proc. Natl. Acad. Sci. USA *107*, 15613–15618. https://doi.org/10.1073/pnas.1007931107.
28. Hallem, E.A., Ho, M.G., and Carlson, J.R. (2004). The molecular basis of odor coding in the *Drosophila* antenna. Cell *117*, 965–979. https://doi.org/10.1016/j.cell.2004.05.012.
29. Kreher, S.A., Kwon, J.Y., and Carlson, J.R. (2005). The molecular basis of odor coding in the *Drosophila* larva. Neuron *46*, 445–456. https://doi.org/10.1016/j.neuron.2005.04.007.
30. Andersson, M.N., Lofstedt, C., and Newcomb, R.D. (2015). Insect olfaction and the evolution of receptor tuning. Front. Ecol. Evol. *3*, 1–13. https://doi.org/10.3389/fevo.2015.00053.
31. Datta, S.R., Vasconcelos, M.L., Ruta, V., Luo, S., Wong, A., Demir, E., Flores, J., Balonze, K., Dickson, B.J., and Axel, R. (2008). The *Drosophila* pheromone cVA activates a sexually dimorphic neural circuit. Nature *452*, 473–477. https://doi.org/10.1038/nature06808.
32. Hansson, B.S., Ljungberg, H., Hallberg, E., and Löfstedt, C. (1992). Functional specialization of olfactory glomeruli in a moth. Science *256*, 1313–1315. https://doi.org/10.1126/science.1598574.

Please cite this article in press as: Jiang et al., Ring-shaped odor coding in the antennal lobe of migratory locusts, Cell (2024), https://doi.org/10.1016/j.cell.2024.05.036

33. Haverkamp, A., Hansson, B.S., and Knaden, M. (2018). Combinatorial codes and labeled lines: how insects use olfactory cues to find and Judge Food, mates, and oviposition sites in complex environments. Front. Physiol *9*, 49. https://doi.org/10.3389/fphys.2018.00049.

34. Hart, T., Frank, D.D., Lopes, L.E., Olivos-Cisneros, L., Lacy, K.D., Trible, W., Ritger, A., Valdés-Rodríguez, S., and Kronauer, D.J.C. (2023). Sparse and stereotyped encoding implicates a core glomerulus for ant alarm behavior. Cell *186*, 3079–3094.e17. https://doi.org/10.1016/j.cell.2023.05.025.

35. Ramaekers, A., Magnenat, E., Marin, E.C., Gendre, N., Jefferis, G.S.X.E., Luo, L.Q., and Stocker, R.F. (2005). Glomerular maps without cellular redundancy at successive levels of the *Drosophila* larval olfactory circuit. Curr. Biol. *15*, 982–992. https://doi.org/10.1016/j.cub.2005.04.032.

36. Riesgo-Escovar, J., Woodard, C., Gaines, P., and Carlson, J. (1992). Development and organization of the *Drosophila* olfactory system: an analysis using enhancer traps. J. Neurobiol. *23*, 947–964. https://doi.org/10.1002/neu.480230803.

37. Godino, L.L.P., and Bate, M. (2009). Embryonic development of the larval olfactory system in *Drosophila*. J. Neurogenet. *23*, S58.

38. Torto, B., Obeng-Ofori, D., Njagi, P.G.N., Hassanali, A., and Amiani, H. (1994). Aggregation pheromone system of adult gregarious desert locust schistocerca gregaria (forskal). J. Chem. Ecol. *20*, 1749–1762. https://doi.org/10.1007/BF02059896.

39. Ferenz, H.J., and Seidelmann, K. (2003). Pheromones in relation to aggregation and reproduction in desert locusts. Physiol. Entomol. *28*, 11–18. https://doi.org/10.1046/j.1365-3032.2003.00318.x.

40. Torto, B., Njagi, P.G.N., Hassanali, A., and Amiani, H. (1996). Aggregation pheromone system of nymphal gregarious desert locust, *Schistocerca gregaria* (forskål). J. Chem. Ecol. *22*, 2273–2281. https://doi.org/10.1007/BF02029546.

41. Dillon, R.J., Vennard, C.T., and Charnley, A.K. (2000). Exploitation of gut bacteria in the locust. Nature *403*, 851. https://doi.org/10.1038/35002669.

42. Guo, X.J., Yu, Q.Q., Chen, D.F., Wei, J.N., Yang, P.C., Yu, J., Wang, X.H., and Kang, L. (2020). 4-Vinylanisole is an aggregation pheromone in locusts. Nature *584*, 584–588. https://doi.org/10.1038/s41586-020-2610-4.

43. Yang, J., Yu, Q., Yu, J., Kang, L., and Guo, X. (2023). 4-Vinylanisole promotes conspecific interaction and acquisition of gregarious behavior in the migratory locust. Proc. Natl. Acad. Sci. USA *120*, e2306659120. https://doi.org/10.1073/pnas.2306659120.

44. Wang, X.H., Fang, X.D., Yang, P.C., Jiang, X.T., Jiang, F., Zhao, D.J., Li, B.L., Cui, F., Wei, J.N., Ma, C.A., et al. (2014). The locust genome provides insight into swarm formation and long-distance flight. Nat. Commun. *5*, 2957. https://doi.org/10.1038/ncomms3957.

45. Wang, Z.F., Yang, P.C., Chen, D.F., Jiang, F., Li, Y., Wang, X.H., and Kang, L. (2015). Identification and functional analysis of olfactory receptor family reveal unusual characteristics of the olfactory system in the migratory locust. Cell. Mol. Life Sci. *72*, 4429–4443. https://doi.org/10.1007/s00018-015-2009-9.

46. Chang, H., Unni, A., Tom, M.T., Llorca, L.C., Brase, S., Bucks, S., Weniger, K., Bisch-Knaden, S., Hansson, B.S., and Knaden, M. (2022). Non-redundant odorant detection in a locust. Preprint at bioRxiv. https://doi.org/10.1101/2022.06.21.496967.

47. Chang, H.T., Cassau, S., Krieger, J., Guo, X.J., Knaden, M., Kang, L., and Hansson, B.S. (2023). A chemical defense deters cannibalism in migratory locusts. Science *380*, 537–543. https://doi.org/10.1126/science.ade6155.

48. Yoritsune, A., and Aonuma, H. (2012). The anatomical pathways for antennal sensory information in the central nervous system of the cricket, *Gryllus bimaculatus*. Invert. Neurosci. *12*, 103–117. https://doi.org/10.1007/s10158-012-0137-6.

49. Paoli, M., Nishino, H., Couzin-Fuchs, E., and Galizia, C.G. (2020). Coding of odour and space in the hemimetabolous insect *Periplaneta americana*. J. Exp. Biol. *223*, jeb218032. https://doi.org/10.1242/jeb.218032.

50. Nishino, H., Iwasaki, M., Paoli, M., Kamimura, I., Yoritsune, A., and Mizunami, M. (2018). Spatial receptive fields for odor localization. Curr. Biol. *28*, 600–608.e3. https://doi.org/10.1016/j.cub.2017.12.055.

51. Ignell, R., Anton, S., and Hansson, B.S. (2001). The antennal lobe of Orthoptera - Anatomy and evolution. Brain Behav. Evol. *57*, 1–17. https://doi.org/10.1159/000047222.

52. Anton, S., Ignell, R., and Hansson, B.S. (2002). Developmental changes in the structure and function of the central olfactory system in gregarious and solitary desert locusts. Microsc. Res. Tech. *56*, 281–291. https://doi.org/10.1002/jemt.10032.

53. Pregitzer, P., Jiang, X.C., Grosse-Wilde, E., Breer, H., Krieger, J., and Fleischer, J. (2017). In search for pheromone receptors: certain members of the odorant receptor family in the desert locust *Schistocerca gregaria* (Orthoptera: Acrididae) are co-expressed with SNMP1. Int. J. Biol. Sci. *13*, 911–922. https://doi.org/10.7150/ijbs.18402.

54. Bazhenov, M., Stopfer, M., Rabinovich, M., Huerta, R., Abarbanel, H.D.I., Sejnowski, T.J., and Laurent, G. (2001). Model of transient oscillatory synchronization in the locust antennal lobe. Neuron *30*, 553–567. https://doi.org/10.1016/S0896-6273(01)00284-7.

55. Mazor, O., and Laurent, G. (2005). Transient dynamics versus fixed points in odor representations by locust antennal lobe projection neurons. Neuron *48*, 661–673. https://doi.org/10.1016/j.neuron.2005.09.032.

56. Cassenaer, S., and Laurent, G. (2012). Conditional modulation of spike-timing-dependent plasticity for olfactory learning. Nature *482*, 47–52. https://doi.org/10.1038/nature10776.

57. Kim, B., Haney, S., Milan, A.P., Joshi, S., Aldworth, Z., Rulkov, N., Kim, A.T., Bazhenov, M., and Stopfer, M.A. (2023). Olfactory receptor neurons generate multiple response motifs, increasing coding space dimensionality. eLife *12*, e79152. https://doi.org/10.7554/eLife.79152.

58. Sun, K., Ray, S., Gupta, N., Aldworth, Z., and Stopfer, M. (2024). Olfactory system structure and function in newly hatched and adult locusts. Sci. Rep. *14*, 2608. https://doi.org/10.1038/s41598-024-52879-7.

59. Petelski, I., Günzel, Y., Sayin, S., Kraus, S., and Couzin-Fuchs, E. (2023). Synergistic olfactory processing for social plasticity in desert locusts. Preprint at bioRxiv. https://doi.org/10.1101/2023.09.15.557953.

60. Ignell, R., Anton, S., and Hansson, B.S. (1999). Integration of behaviourally relevant odours at the central nervous level in solitary and gregarious third instar locusts, *Schistocerca gregaria*. J. Insect Physiol. *45*, 993–1000. https://doi.org/10.1016/S0022-1910(99)00080-3.

61. Zhao, Z.L., Zung, J.L., Hinze, A., Kriete, A.L., Iqbal, A., Younger, M.A., Matthews, B.J., Merhof, D., Thiberge, S., Ignell, R., et al. (2022). Mosquito brains encode unique features of human odour to drive host seeking. Nature *605*, 706–712. https://doi.org/10.1038/s41586-022-04675-4.

62. Carcaud, J., Otte, M., Grünewald, B., Haase, A., Sandoz, J.C., and Beye, M. (2023). Multisite imaging of neural activity using a genetically encoded calcium sensor in the honey bee. PLOS Biol. *21*, e3001984. https://doi.org/10.1371/journal.pbio.3001984.

63. Doudna, J.A., and Charpentier, E. (2014). Genome editing. The new frontier of genome engineering with CRISPR-Cas9. Science *346*, 1258096. https://doi.org/10.1126/science.1258096.

64. Ran, F.A., Hsu, P.D., Wright, J., Agarwala, V., Scott, D.A., and Zhang, F. (2013). Genome engineering using the CRISPR-Cas9 system. Nat. Protoc. *8*, 2281–2308. https://doi.org/10.1038/nprot.2013.143.

65. Hsu, P.D., Lander, E.S., and Zhang, F. (2014). Development and applications of CRISPR-Cas9 for genome engineering. Cell *157*, 1262–1278. https://doi.org/10.1016/j.cell.2014.05.010.

66. Li, Y., Zhang, J., Chen, D.F., Yang, P.C., Jiang, F., Wang, X.H., and Kang, L. (2016). CRISPR-Cas9 in locusts: successful establishment of an olfactory deficiency line by targeting the mutagenesis of an odorant receptor

Please cite this article in press as: Jiang et al., Ring-shaped odor coding in the antennal lobe of migratory locusts, Cell (2024), https://doi.org/10.1016/j.cell.2024.05.036

co-receptor (Orco). Insect Biochem. Mol. Biol. *79*, 27–35. https://doi.org/10.1016/j.ibmb.2016.10.003.

67. Yang, Y., Krieger, J., Zhang, L., and Breer, H. (2012). The Olfactory Co-receptor Orco from the Migratory Locust (*Locusta migratoria*) and the Desert Locust (*Schistocerca gregaria*): Identification and Expression pattern. Int. J. Biol. Sci. *8*, 159–170. https://doi.org/10.7150/ijbs.8.159.
68. Tian, L., Hires, S.A., Mao, T., Huber, D., Chiappe, M.E., Chalasani, S.H., Petreanu, L., Akerboom, J., McKinney, S.A., Schreiter, E.R., et al. (2009). Imaging neural activity in worms, flies and mice with improved GCaMP calcium indicators. Nat. Methods *6*, 875–881. https://doi.org/10.1038/nmeth.1398.
69. Jiang, X.C., Breer, H., and Pregitzer, P. (2019). Sensilla-specific expression of odorant receptors in the desert locust *Schistocerca gregaria*. Front. Physiol. *10*, 1052. https://doi.org/10.3389/fphys.2019.01052.
70. Riabinina, O., Task, D., Marr, E., Lin, C.C., Alford, R., O'Brochta, D.A., and Potter, C.J. (2016). Organization of olfactory centres in the malaria mosquito *Anopheles gambiae*. Nat. Commun. *7*, 13010. https://doi.org/10.1038/ncomms13010.
71. Guo, M., Krieger, J., Grosse-Wilde, E., Missbach, C., Zhang, L., and Breer, H. (2014). Variant ionotropic receptors are expressed in olfactory sensory neurons of coeloconic sensilla on the antenna of the desert locust (*Schistocerca gregaria*). Int. J. Biol. Sci. *10*, 1–14. https://doi.org/10.7150/ijbs.7624.
72. Maresh, A., Rodriguez Gil, D.R., Whitman, M.C., and Greer, C.A. (2008). Principles of glomerular organization in the human olfactory bulb-implications for odor processing. PLoS One *3*, e2640. https://doi.org/10.1371/journal.pone.0002640.
73. Miyasaka, N., Arganda-Carreras, I., Wakisaka, N., Masuda, M., Sümbül, U., Seung, H.S., and Yoshihara, Y. (2014). Olfactory projectome in the zebrafish forebrain revealed by genetic single-neuron labelling. Nat. Commun. *5*, 3639. https://doi.org/10.1038/ncomms4639.
74. Weiss, L., Jungblut, L.D., Pozzi, A.G., O'Connell, L.A., Hassenklöver, T., and Manzini, I. (2020). Conservation of glomerular organization in the main olfactory bulb of anuran larvae. Front. Neuroanat. *14*, 44. https://doi.org/10.3389/fnana.2020.00044.
75. Heinze, S., El Jundi, B., Berg, B.G., Homberg, U., Menzel, R., Pfeiffer, K., Hensgen, R., Zittrell, F., Dacke, M., Warrant, E., et al. (2021). A unified platform to manage, share, and archive morphological and functional data in insect neuroscience. eLife *10*, e65376. https://doi.org/10.7554/eLife.65376.
76. Knaden, M., Strutz, A., Ahsan, J., Sachse, S., and Hansson, B.S. (2012). Spatial representation of odorant valence in an insect brain. Cell Rep. *1*, 392–399. https://doi.org/10.1016/j.celrep.2012.03.002.
77. De Meo, P., Ferrara, E., Fiumara, G., and Provetti, A. (2011). Generalized Louvain Method for Community Detection in Large Networks (IEEE Publications), pp. 88–93. https://doi.org/10.1109/ISDA.2011.6121636.
78. Demsar, J., Curk, T., Erjavec, A., Gorup, C., Hocevar, T., Milutinovic, M., Mozina, M., Polajnar, M., Toplak, M., Staric, A., et al. (2013). Orange: data mining toolbox in Python. J. Mach. Learn. Res. *14*, 2349–2353.
79. Que, X.Y., Checconi, F., Petrini, F., and Gunnels, J.A. (2015). Scalable community detection with the Louvain algorithm. Int. Parall. Distrib. P., 28–37. https://doi.org/10.1109/IPDPS.2015.59.
80. Anton, S., and Hansson, B.S. (1996). Antennal lobe interneurons in the desert locust *Schistocerca gregaria* (Forskal): processing of aggregation pheromones in adult males and females. J. Comp. Neurol. *370*, 85–96. https://doi.org/10.1002/(SICI)1096-9861(19960617)370:1<85::AID-CNE8>3.0.CO;2-H.
81. Strausfeld, N.J., and Hildebrand, J.G. (1999). Olfactory systems: common design, uncommon origins? Curr. Opin. Neurobiol. *9*, 634–639. https://doi.org/10.1016/S0959-4388(99)00019-7.
82. Mombaerts, P. (2006). Axonal wiring in the mouse olfactory system. Annu. Rev. Cell Dev. Biol. *22*, 713–737. https://doi.org/10.1146/annurev.cellbio.21.012804.093915.
83. Belluscio, L., Lodovichi, C., Feinstein, P., Mombaerts, P., and Katz, L.C. (2002). Odorant receptors instruct functional circuitry in the mouse olfactory bulb. Nature *419*, 296–300. https://doi.org/10.1038/nature01001.
84. Wong, A.M., Wang, J.W., and Axel, R. (2002). Spatial representation of the glomerular map in the *Drosophila* protocerebrum. Cell *109*, 229–241. https://doi.org/10.1016/s0092-8674(02)00707-9.
85. Gao, Q., Yuan, B.B., and Chess, A. (2000). Convergent projections of olfactory neurons to specific glomeruli in the antennal lobe. Nat. Neurosci. *3*, 780–785. https://doi.org/10.1038/77680.
86. Murthy, V.N. (2011). Olfactory maps in the brain. Annu. Rev. Neurosci. *34*, 233–258. https://doi.org/10.1146/annurev-neuro-061010-113738.
87. Zou, D.J., Chesler, A., and Firestein, S. (2009). How the olfactory bulb got its glomeruli: a just so story? Nat. Rev. Neurosci. *10*, 611–618. https://doi.org/10.1038/nrn2666.
88. Berck, M.E., Khandelwal, A., Claus, L., Hernandez-Nunez, L., Si, G.W., Tabone, C.J., Li, F., Truman, J.W., Fetter, R.D., Louis, M., et al. (2016). The wiring diagram of a glomerular olfactory system. eLife *5*, e14859. https://doi.org/10.7554/eLife.14859.
89. Weigand, M., Sartori, F., and Cuntz, H. (2017). Universal transition from unstructured to structured neural maps. Proc. Natl. Acad. Sci. USA *114*, E4057–E4064. https://doi.org/10.1073/pnas.1616163114.
90. Kaschube, M. (2014). Neural maps versus salt-and-pepper organization in visual cortex. Curr. Opin. Neurobiol. *24*, 95–102. https://doi.org/10.1016/j.conb.2013.08.017.
91. Bazhenov, M., Stopfer, M., Rabinovich, M., Abarbanel, H.D.I., Sejnowski, T.J., and Laurent, G. (2001). Model of cellular and network mechanisms for odor-evoked temporal patterning in the locust antennal lobe. Neuron *30*, 569–581. https://doi.org/10.1016/S0896-6273(01)00286-0.
92. Offner, T., Weiss, L., Daume, D., Berk, A., Inderthal, T.J., Manzini, I., and Hassenklöver, T. (2023). Functional odor map heterogeneity is based on multifaceted glomerular connectivity in larval olfactory bulb. iScience *26*, 107518. https://doi.org/10.1016/j.isci.2023.107518.
93. Fisher, Y.E. (2022). Flexible navigational computations in the central complex. Curr. Opin. Neurobiol. *73*, 102514. https://doi.org/10.1016/j.conb.2021.12.001.
94. Plath, J.A., and Barron, A.B. (2015). Current progress in understanding the functions of the insect central complex. Curr. Opin. Insect Sci. *12*, 11–18. https://doi.org/10.1016/j.cois.2015.08.005.
95. Omoto, J.J., Nguyen, B.M., Kandimalla, P., Lovick, J.K., Donlea, J.M., and Hartenstein, V. (2018). Neuronal Constituents and Putative Interactions Within the Ellipsoid Body Neuropil. Front. Neural Circuits *12*, 103. https://doi.org/10.3389/fncir.2018.00103.
96. Pfeiffer, K., and Homberg, U. (2014). Organization and functional roles of the central complex in the insect brain. Annu. Rev. Entomol. *59*, 165–184-U787. https://doi.org/10.1146/annurev-ento-011613-162031.
97. Marin, E.C., Jefferis, G.S.X.E., Komiyama, T., Zhu, H., and Luo, L. (2002). Representation of the glomerular olfactory map in the *Drosophila* brain. Cell *109*, 243–255. https://doi.org/10.1016/s0092-8674(02)00700-6.
98. Choi, K., Kim, W.K., and Hyeon, C. (2022). Olfactory responses of are encoded in the organization of projection neurons. eLife *11*, e77748. https://doi.org/10.7554/eLife.77748.
99. Perez-Orive, J., Mazor, O., Turner, G.C., Cassenaer, S., Wilson, R.I., and Laurent, G. (2002). Oscillations and sparsening of odor representations in the mushroom body. Science *297*, 359–365. https://doi.org/10.1126/science.1070502.
100. Broussard, G.J., Liang, Y.J., Fridman, M., Unger, E.K., Meng, G.H., Xiao, X., Ji, N., Petreanu, L., and Tian, L. (2018). In vivo measurement of afferent activity with axon-specific calcium imaging. Nat. Neurosci. *21*, 1272–1280. https://doi.org/10.1038/s41593-018-0211-4.
101. Yang, Q.P., Li, Z., Cao, J.J., Zhang, S.D., Zhang, H.J., Wu, X.Y., Zhang, Q.W., and Liu, X.X. (2014). Selection and assessment of reference genes for quantitative PCR normalization in migratory locust *Locusta migratoria*

Please cite this article in press as: Jiang et al., Ring-shaped odor coding in the antennal lobe of migratory locusts, Cell (2024), https://doi.org/10.1016/j.cell.2024.05.036

(Orthoptera: Acrididae). PLoS One *9*, e98164. https://doi.org/10.1371/journal.pone.0098164.

102. Ott, S.R. (2008). Confocal microscopy in large insect brains: zinc-formaldehyde fixation improves synapsin immunostaining and preservation of morphology in whole-mounts. J. Neurosci. Meth. *172*, 220–230. https://doi.org/10.1016/j.jneumeth.2008.04.031.

103. Mohamed, A.A.M., Retzke, T., Das Chakraborty, S., Fabian, B., Hansson, B.S., Knaden, M., and Sachse, S. (2019). Odor mixtures of opposing valence unveil inter-glomerular crosstalk in the *Drosophila* antennal lobe. Nat. Commun. *10*, 1201. https://doi.org/10.1038/s41467-019-09069-1.

104. Haddad, R., Khan, R., Takahashi, Y.K., Mori, K., Harel, D., and Sobel, N. (2008). A metric for odorant comparison. Nat. Methods *5*, 425–429. https://doi.org/10.1038/Nmeth.1197.

Please cite this article in press as: Jiang et al., Ring-shaped odor coding in the antennal lobe of migratory locusts, Cell (2024), https://doi.org/10.1016/j.cell.2024.05.036

STAR★METHODS

KEY RESOURCES TABLE

REAGENT or RESOURCE	SOURCE	IDENTIFIER
Antibodies		
Rabbit Polyclonal anti- GFP	Invitrogen	Catalog # A-11122; RRID: AB_221569
Mouse monoclonal anti-SYNORF1	Developmental Systems Hybridoma Bank	DSHB: 3C11; RRID: AB_528479
Goat anti-Rabbit Alexa Fluor 488	Invitrogen	Catalog # A-11008; RRID: AB_143165
Goat anti-Mouse Alexa Fluor 546	Invitrogen	Catalog # A-11030; RRID: AB_2534089
Rabbit Polyclonal anti-GFP, Alexa Fluor 488	Invitrogen	Catalog # A-21311; RRID: AB_221477
Chemicals, peptides, and recombinant proteins		
L-alpha-Terpineol	Sigma-Aldrich	W304522, Cas:10482-56-1
Phenylacetonitrile	Sigma-Aldrich	B19401, Cas: 140-29-4
Geranyl acetone	FLUKA	48805, Cas: 3796-70-1
2-Methyl-5-isopropylpyrazine	BOC sciences	BCH12929-2, Cas: 13925-05-8
Limonene	Sigma-Aldrich	W524905, Cas: 138-86-3
1,3-Dimethyluracil	TCI	D0808, Cas: 874-14-6
gamma-Caprolactone	Sigma-Aldrich	W255602, Cas: 695-06-7
Isophorone	Sigma-Aldrich	w355305, Cas:78-59-1
Linalool oxide	FLUKA	62141, Cas: 60047-17-8
Indole	Sigma-Aldrich	I3408, Cas: 120-72-9
(+/−)-Linalool	Sigma-Aldrich	L2602, Cas: 78-70-6
Dihydroactinidiolide	BOC sciences	BCR24823-1A, Cas: 17092-92-1
Acetophenone	Sigma-Aldrich	42163, Cas: 98-86-2
2,4,6-Trimethylpyridine	Sigma-Aldrich	27690, Cas: 108-75-8
Decanal	Sigma-Aldrich	D7384, Cas: 112-31-2
(E)-2-Octen-1-ol	Sigma-Aldrich	547115, Cas: 18409-17-1
4-Vinylanisole	Sigma-Aldrich	141003, Cas: 637-69-4
trans-2-Hexen-1-ol	FLUKA	53057, Cas: 928-95-0
α-Pinene oxide	Sigma-Aldrich	218308, Cas: 1686-14-2
Ethyl hexanoate	Sigma-Aldrich	148962, Cas: 123-66-0
Benzyl alcohol	FLUKA	08421, Cas: 100-51-6
1-Pentanol	Sigma-Aldrich	138975, Cas: 71-41-0
Guaiacol	Sigma-Aldrich	W253200, Cas: 90-05-1
2,5-Dimethyl-pyrazine	Sigma-Aldrich	W327204, Cas: 123-32-0
Phenethyl alcohol	FLUKA	77861, Cas: 60-12-8
2-heptanone	Sigma-Aldrich	w254401, Cas: 110-43-0
Benzaldehyde	ACROS	378361000, Cas: 100-52-7
Anisole	FLUKA	96109, Cas: 100-66-3
Veratrole	Sigma-Aldrich	140155, Cas: 91-16-7
Octanal	Sigma-Aldrich	O5608, Cas:124-13-0
Phenylacetaldehyde	Sigma-Aldrich	107395, Cas: 122-78-1
Hexanoic acid	Sigma-Aldrich	153745, Cas: 142-62-1
1-octen-3-ol	SAFC	w280518, Cas: 3391-86-4
Butyl acetate	FLUKA	45860, Cas: 123-86-4
(E)-2-hexenal	ACROS	158130250, Cas: 6728-26-3
2,4,dimethoxyphenol	Sigma-Aldrich	SY3H3D67C12, Cas: 13330-65-9

(*Continued on next page*)

Please cite this article in press as: Jiang et al., Ring-shaped odor coding in the antennal lobe of migratory locusts, Cell (2024), https://doi.org/10.1016/j.cell.2024.05.036

Continued

REAGENT or RESOURCE	SOURCE	IDENTIFIER
1-Butoxy-2-propanol	TCI	B0864, Cas: 5131-66-8
Decane	Fischer scientific	15617840, Cas: 124-18-5
DEET	Sigma-Aldrich	36542, Cas: 134-62-3
(±)-Geosmin	Sigma-Aldrich	UC18, CAS: 16423-19-1
2-Methylbutyric acid	TCI	H1296, Cas: 116-53-0
2-Ethylhexyl acetate	Sigma-Aldrich	W514705, Cas: 103-09-3
Diacetone alcohol	Sigma-Aldrich	H41544, Cas: 123-42-2
Squalene	Sigma-Aldrich	S3626, Cas: 111-02-4
Methyl oleate	Sigma-Aldrich	311111, Cas: 112-62-9
Linoleic acid	FLUKA	62230, Cas: 60-33-3
Neurobiotin	Vector Laboratories	SP-1120
VECTASHIELD Antifade Mounting Medium	Vector Laboratories	H-1000-10
Streptavidin, DyLight 549	Vector Laboratories	SA-5549-1
sgRNA	IDT	N/A
Alt-R S.p. Cas9 Nuclease V3, 100 μg	IDT	1081058
Dextran, Tetramethylrhodamine and biotin, (micro-Ruby)	Invitrogen	D7162
Normal Goat Serum	Sigma-Aldrich	NS02L
RapiClear 1.52	SUNJIN Lab	#RC152001
Critical commercial assays		
Genotyping kit: MyTaq HS Red DNA Polymerase	Meridian Bioscience Inc.	BIO-21115
Plasmid extraction kit: NucleoBond Xtra Midi EF	Macherey Nagel	REF 740420.50
Gibson assembly kit: NEBuilder HiFi DNA Assembly Master Mix	New England Biolabs Inc.	E2621S
PCR: Q5 High-Fidelity DNA Polymerase	New England Biolabs Inc.	M0491S
Sequencing: Eurofins Mix2Seq Kit	Eurofins	N/A
qPCR: Biozym Blue S'Green qPCR Mix Separate ROX	Biozym, Steinbrinksweg	331416S
Deposited data		
Raw, plot and analysis data	Edmond	https://edmond.mpg.de/dataset.xhtml?persistentId=doi:10.17617/3.JQF9GL&version=DRAFT
Oligonucleotides		
Orco_LHA_F: CAAGGTCGTCCGATTGAACA	This paper	N/A
Orco_RHA_R: AATGTCCGAAAGATGACGCT	This paper	N/A
T2A_GCaMP6_overhang_F: CATGGTGCTG GTGCAGCTCAAGGGAGAGGGCAGAGGAAGTC	This paper	N/A
T2A_GCaMP_overhang_R GCGCTGACGTCAC AGGCGCCTATCACTTCGCTGTCATCATTTGT	This paper	N/A
T2A_GCaMP6_backbone_F: TAGGCGCCTGT GACGTCAGCGCCG	This paper	N/A
T2A_GCaMP6_backbone_R: CTTGAGCTGCA CCAGCACCATGAAG	This paper	N/A
sgRNA_LHA_F: CCTACTTGAGCTGCACCAG CACCAATGTCCGAAAGATGACGCT	This paper	N/A
sgRNA_RHA_R: GGTGCTGGTGCAGCTCAA GTAGGCAAGGTCGTCCGATTGAACA	This paper	N/A
Backbone_F: ATGGGTTCTCATCATCATCATCATCA	This paper	N/A
Backbone_R: AGGGCCGGGATTCTCCTCCA	This paper	N/A

(*Continued on next page*)

Continued

REAGENT or RESOURCE	SOURCE	IDENTIFIER
T2A_Syn_overhang_F: TGACGTGGAGGAGAATC CCGGCCCTATGGACGTGGTGAATCAGCT	This paper	N/A
Syn_GSG_R: GGAGCCGGAGCCCGATCCCA TCTGATTGGAGAAGGAGGTGG	This paper	N/A
Syn_GCaMP6_overhang_R: GATGATGATGA TGATGAGAACCCATGGAGCCGGAGCCCGAT	This paper	N/A
Orco-T2A-GCaMP6_F: CCTTACGTATATGGGTGGTTCTTA	This paper	N/A
Orco-T2A-GCaMP6_R: CTTATTCCACTTACGACGTGATG	This paper	N/A
Orco-Syn-GCaMP6_F: CCTTACGTATATGGGTGGTTCTTA	This paper	N/A
Orco-Syn-GCaMP6_R: CACTCTCCGTCTTGTTGGCA	This paper	N/A
OR70a_promoter_F: AGATGGTGTTAATTTTATCGTGAGC	This paper	N/A
OR70a_promoter_R: CTGGACGTCTGCACGAAACTAA	This paper	N/A
mCD8-mCherry_backbone_F: CTCCCTGGTTTAGTTTC GTGCAGACGTCCAGATGGCCTCACCGTTGACCCGCTTTC	This paper	N/A
mCD8-mCherry_backbone_R: AGTGTGATGGATATCTG CAGAATTCGCCCTTAACTTGTTTATTGCAGCTTATAATGG	This paper	N/A
OR70a-mCherry_F: ATGGCCTCACCGTTGACCCGCT	This paper	N/A
OR70a-mCherry_R: TTGGTCACCTTCAGCTTGGCG	This paper	N/A
GCaMP6s_qPCR_S:ATCAAGGCCGACAAGCAGAA	This paper	N/A
GCaMP6s_qPCR_AS: CACGCTCAGGTAGTGGTTGT	This paper	N/A
EF1α_S:: AGCCCAGGAGATGGGTAAAG	This paper	N/A
EF1α_AS: CTCTGTGGCCTGGAGCATC	This paper	N/A
Recombinant DNA		
15x-QUAS-dTomato-T2A-GCaMP6s	Addgene	#130666
pAAV-Ef1a-DIO-Synaptophysin-GCaMP6s	Addgene	#105715
slc1a3b:mCD8mCherry	Addgene	#170207
Software and algorithms		
Fiji	National Institutes of Health	https://imagej.net/software/fiji/
Origin 2023b	OriginLab Corporation	https://www.originlab.com/getstarted
Chopchop	University of Bergen	https://chopchop.cbu.uib.no/
ZEN 3.4 blue edition	ZEISS	https://www.zeiss.com/microscopy/en/products/software/zeiss-zen.html
TurboReg	Biomedical Imaging Group - EPFL	http://bigwww.epfl.ch/thevenaz/turboreg/
StackReg	Biomedical Imaging Group - EPFL	http://bigwww.epfl.ch/thevenaz/stackreg/
AMIRA 5.5.0	Thermo Fisher Scientific	https://www.thermofisher.com/de/de/home/electron-microscopy/products/software-em-3d-vis/amira-software.html
Enhanced data analysis	Agilent	https://www.agilent.com/en/product/software-informatics/mass-spectrometry-software/data-analysis
NIST MS	National Institute of Standards and Technology	https://chemdata.nist.gov/
SNT	Fiji	https://imagej.net/plugins/snt/
Adobe Illustrator	Adobe	https://www.adobe.com/de/products/illustrator.html
LabView	National Instruments	https://www.ni.com/de/support/downloads/software-products/download.labview.html#487445

(*Continued on next page*)

Please cite this article in press as: Jiang et al., Ring-shaped odor coding in the antennal lobe of migratory locusts, Cell (2024), https://doi.org/10.1016/j.cell.2024.05.036

Continued

REAGENT or RESOURCE	SOURCE	IDENTIFIER
ChemDraw	PerkinElmer	https://revvitysignals.com/products/research/chemdraw
Dragon 5.0	TALETE srl	http://www.ccl.net/qsar/archives/0403/0458.html
Segmentation editor	Fiji	https://imagej.net/plugins/segmentation-editor
Orange 3	University of Ljubljana	https://orangedatamining.com/
Geneious Prime	Biomatters	https://www.geneious.com/

RESOURCE AVAILABILITY

Lead contact

Further information and requests for resources and reagents should be directed to and will be fulfilled by the lead contact, Bill Hansson (hansson@ice.mpg.de).

Materials availability

Further information and requests for resources and reagents should be directed to and will be fulfilled by the lead contact.

Data and code availability

All raw data supporting the findings of this study will be made available through Edmond, the Open Access Data Repository of the Max Planck Society upon paper's acceptance. This paper does not report original code. Any additional information required to re-analyze the data reported in this work paper is available from the lead contact upon request.

EXPERIMENTAL MODEL AND STUDY PARTICIPANT DETAILS

Locust husbandry

The locusts (*Locusta migratoria*) used in this study were obtained from the Institute of Zoology, Chinese Academy of Sciences, Beijing, China. They were bred in a well-ventilated climate chamber under controlled conditions, including a temperature of 30°C, 40% humidity, and a day:night ratio of 16 h to 8 h. All locusts used in the experiments were in the gregarious phase. To create a crowded state, approximately 2000 young instar locusts were reared together in a cage measuring 30 cm × 30 cm × 50 cm. The locusts were fed a diet consisting of fresh maize and wheat, supplemented with organic wheat bran.

Generation of a *Orco-GCaMP6s* transgenic locust

Plasmid construction

We leveraged the CRISPR-Cas9 system-mediated homology recombination strategy to site-specifically knock-in the exogeneous gene cassette encoding GCaMP6s. We targeted the last exon of *Orco* (exon 8) and designed single guide RNA that reversely complements a genome domain containing the stop codon (GGTGCTGGTGCAGCTCAAGTAGG, PAM region underscored). We reprogrammed the native transcription event of Orco by linking the Orco coding sequence with the GCaMP6s coding sequence with T2A, a self-cleaving peptide, ensuring the co-localization of Orco and GCaMP6s in olfactory sensory neurons (OSNs) and the undisrupted functionality of Orco.[9,16] This strategy generates the preliminary *Orco-T2A-GCaMP6s* locusts where GCaMP6s was supposed to be expressed homogenously within the cytosol. To enhance GCaMP6s expression in the axon terminals of OSNs in the locust antennal lobe, based on the established construct of *Orco-T2A-GCaMP6s*, we additionally linked the GCaMP6s with a presynaptic-enriched guide protein,[100] resulting in a presynaptic enhanced transgenic version named Orco-Syn-GCaMP6s.

Construction of *Orco-T2A-GCaMP6s* plasmid contained 3 steps:

1. Cloning of Orco-exon 8 flanking sequence. Both homology arms flanking the insertion site are 1kb. Primers:

Orco_LHA_F
CAAGGTCGTCCGATTGAACA
Orco_RHA_R
AATGTCCGAAAGATGACGCT.
The amplicon was cloned into the TOPO blunt vector and assembled plasmid was used as the backbone for step 2.

Please cite this article in press as: Jiang et al., Ring-shaped odor coding in the antennal lobe of migratory locusts, Cell (2024), https://doi.org/10.1016/j.cell.2024.05.036

2. Cloning of T2A_GCaMP6s insertion with the overhang to the backbone based on the plasmid #130666 from addgene. Primers:
T2A_GCaMP6_overhang_F

CATGGTGCTGGTGCAGCTCAAGGGAGAGGGCAGAGGAAGTC
T2A_GCaMP_overhang_R
GCGCTGACGTCACAGGCGCCTATCACTTCGCTGTCATCATTTGT
The primers for cloning backbone (from step 1) were:
T2A_GCaMP6_backbone_F
TAGGCGCCTGTGACGTCAGCGCCG
T2A_GCaMP6_backbone_R
CTTGAGCTGCACCAGCACCATGAAG
The amplicons of insertion and backbone were assembled using Gibson Assembly kit (NEB).

3. Add linearization site with designed short guide RNA flanking both LHA and RHA. Primers:

sgRNA_LHA_F
CCTACTTGAGCTGCACCAGCACCAATGTCCGAAAGATGACGCT
sgRNA_RHA_R
GGTGCTGGTGCAGCTCAAGTAGGCAAGGTCGTCCGATTGAACA
The amplicons were cloned into TOPO XL2 plasmid (Thermo Fisher Scientific) for generation of donor plasmid of Orco-T2A-GCaMP6s.

Construction of *Orco-Syn-GCaMP6s* plasmid in one step:
Cloning of backbone from the constructed plasmid of Orco-T2A-GCaMP6 (above step 3). Primers:
Backbone_F
ATGGGTTCTCATCATCATCATCATCA
Backbone_R
AGGGCCGGGATTCTCCTCCA
Cloning of *Orco-Synaptophysin-GSG-GCaMP6s* insertion with overhang based on the plasmid #105715 from addgene. Primers:
T2A_Syn_overhang_F
TGACGTGGAGGAGAATCCCGGCCCTATGGACGTGGTGAATCAGCT
Syn_GSG_R
GGAGCCGGAGCCCGATCCCATCTGATTGGAGAAGGAGGTGG
Syn_GCaMP6_overhang_R
GATGATGATGATGATGAGAACCCATGGAGCCGGAGCCCGAT
The amplicon was cloned into TOPO XL2 plasmid for generation of donor plasmid of *Orco-Syn-GCaMP6s*.
The reconstructed DNA plasmids were purified using NucleoBond Xtra Midi endotoxin free Kit (Machery Nagel) following manufacture's protocol and were adjusted to proper concentration with nuclease-free water.

Generation of OR70a-mCherry transgenic line:
The generation of *OR70a-mCherry* was derived from the *Orco-Syn-GCaMP6s* transgenic line. Rather than employing site-specific knock-in, we utilized a non-specific knock-in approach for the integration of the OR70a-mCherry gene cassette. Specifically, we amplified the OR70a promoter region, approximately 2.3kb in size, upstream of the start codon based on the published *Locusta migratoria* genome, using the primer:
OR70a_promoter_F
AGATGGTGTTAATTTTATCGTGAGC
OR70a_promoter_R
CTGGACGTCTGCACGAAACTAA
Subsequently, the amplified OR70a promoter was annealed with the reporter gene mCD8-mCherry based on the plasmid #170207 from addgene, using the primer:
mCD8-mCherry_backbone_F
CTCCCTGGTTTAGTTTCGTGCAGACGTCCAGATGGCCTCACCGTTGACCCGCTTTC
mCD8-mCherry_backbone_R
AGTGTGATGGATATCTGCAGAATTCGCCCTTAACTTGTTTATTGCAGCTTATAATGG
To facilitate CRISPR-Cas9-mediated DNA integration, we introduced two synthetic sgRNA cutting sites flanking the OR70a promoter-mCD8-mCherry fragment.

Microinjection

Freshly laid eggs were collected from the egg pods, thoroughly washed with serious of 70% ethanol-Deionized Water for 10 min and were displayed on 1% agarose gel for injection. The injection cocktail contained donor DNA plasmid (600ng/μl), sgRNA (200ng/μl) and Cas9 purified recombination protein (400ng/μl). Both the sgRNA and Cas9 protein were purchased from IDT (Integrated DNA Technologies). 20ul of the injection cocktail was injected into the posterior side of the eggs, where germ cells were developed, using

Nanoliter injector (Waukesha-Pearce Industries, Inc.) with a filamented glass capillary (Sutter Instrument Co.) under a dissection microscope.

Genotyping

The injected eggs were stored in a Petri dish and put in a sterilized plastic container in 30°C chamber for 12-14 days. The mortality rate induced by such microinjection was about 50%. G0 animals at the 5th instar were genotyped for possible DNA integration following the protocol.[42] In brief, the tarsus of the middle leg was scissored and lysed with 45 μl NaOH buffer (50 mM) at 95 °C in a PCR machine for 30 min, neutralized by 5 μl Tris-HCL (pH 8.0, 1 M). We used 1μl of upper supernatant for the subsequent genotyping PCR using MyTaq HS Red kit (Bioline) following a PCR protocol recommended by the manufacture. The PCR amplicon was sequenced for site-specific insertion (Eurofins Mis2Seq DNA sequencing), using the following primers:

Orco-T2A-GCaMP6s:
Orco-T2A-GCaMP6s_F: CCTTACGTATATGGGTGGTTCTTA
Orco-T2A-GCaMP6s_R: CTTATTCCACTTACGACGTGATG
Orco-Syn-GCaMP6s:
Orco-Syn-GCaMP6s_F: CCTTACGTATATGGGTGGTTCTTA
Orco-Syn-GCaMP6s_R: CACTCTCCGTCTTGTTGGCA
OR70a-mCherry_F:
ATGGCCTCACCGTTGACCCGCT
OR70a-mCherry_R:
TTGGTCACCTTCAGCTTGGCG

The numbers of injected embryos and detected gene integrations are listed as follows:

Transgenic line	Embryo injection	Hatched embryo	Genotyped locust	Genotyped positive locust
Orco-GCaMP6s	1998	249	189	2
Orco-Syn-GCaMP6s	2120	260	196	1
OR70a-mCherry	698	98	70	55

Husbandry

We obtained one male and one female locust for *Orco-T2A-GCaMP6s* and one female locust for *Orco-T2A-Syn-GCaMP6s*, with the homology recombination rate lower than 1%. The validated G0 locust was paired with a WT locust to generate offspring. In the next generation, screening of the heterozygous offspring followed the genotyping protocol mentioned above. For both genotypes, G1 animals were detective of a site-specific insertion with the heterozygous locusts less than half of the population. The validated locusts were then in-crossed for the G2 offspring, which were subject to the same genotyping procedure for homozygous locusts using the primer:

Homo-F:
ATCACCCGGTATGGTCGTTTACA
Homo-R:
ATACTACACCCTGAAACACCC

The obtained homozygous *Orco-Syn-GCaMP6s* locusts were inbreeded for at least 5 generations before used for the experiments. The *OR70a-mCherry* locusts identified as positive for gene insertion through screening were grouped for mating to produce offspring. Immunostaining of *OR70a-mCherry* was performed in the second generation.

Phenotypic inspection

For phenotypic inspection, one adult locust's antenna was extracted and briefly drenched in nuclease-free water. The antenna was then press mounted on a glass slide containing spread dental wax. The antenna was split longitudinally into two halves with a sharp blazer and was embedded with Vectashield (Vector Laboratories) to protect the fluorescence from distinction. The endogenous GFP fluorescence was inspected through confocal microscopy (Zeiss LSM 880) using the LAMDA scanning mode and the autofluorescence from cuticle and other non-cellular items was unmixed online.

Real-time quantitative PCR

RNA extraction was performed treating dissected locust central brains from stage 1 to stage 6 with the TRIzol reagent (Invitrogen, Waltham, MA, USA) following the recommend protocol from the manufacture. To compensate for the developmental-induced increase in brain size, the number of central brains used was reduced from seven in stage 1 to two in stage 6, respectively. The extracted RNA was subjected to DNaseI (Thermo Fisher Scientific, Waltham, MA, USA) treatment to eliminate genomic DNA contamination. cDNA was synthesized with SuperScript III Reverse transcriptase kits (Invitrogen) using the RNA at a concentration of 125ng/μl. Real-time quantitative PCR was performed to compare the transcript level of GCaMP6s in locust central brains across developmental stages by using Biozym Blue S'Green qPCR Mix Separate ROX (Biozym, Steinbrinksweg, Germany). The elongation factor 1 alpha gene (*ef1α*) was used as a housekeep gene.[101]

The primer used were:
GCaMP6s_qPCR_S:
ATCAAGGCCGACAAGCAGAA
GCaMP6s_qPCR_AS:
CACGCTCAGGTAGTGGTTGT
EF1α_S:
AGCCCAGGAGATGGGTAAAG
EF1α_AS:
CTCTGTGGCCTGGAGCATC

METHOD DETAILS

Locust antennal lobe reconstructions

Immunostaining

Immunostainings of locust brains followed the established protocol with slight modifications.[102] Locust brains were exposed and dissected out of the capsule with adherent tissues and pigmentation on the optic lobe removed. Extracted locust brains were rinsed in locust saline buffer (150 mM NaCl, 5 mM KCl, 5 mM $CaCl_2$, 4 mM $NaHCO_3$, 2 mM $MgCl_2$, 10 mM Hepes and 25 mM sucrose, adjusted to pH 7.1) for 10 min. The brain was fixed in ZnFA at room temperature for 20 h. The ZnFA fixative contained 0.25% (18.4 mM) $ZnCl_2$, 0.788% (135 mM) NaCl, 1.2% (35 mM) sucrose, 1% formaldehyde and 0.1% DMSO. Fixed brains were rinsed in saline buffer for 3x 15 min followed by a standard dehydrate-rehydrate process with an ethanol series of 30%, 50%, 70%, 90%, 96% and 100%, with 10 min each. The brains were then treated with blocking buffer (5% NGS, 1% DMSO, 0.005% NaN_3 in 0.1 M PBS) for 1h at room temperature, which was then replaced with primary antibodies (rabbit anti-GFP and mouse anti-Synapsin) diluted in the blocking buffer at 1:500, lasting for 4 days at room temperature. The brains were rinsed in PBS-DMSO for 3x 45 min and treated with secondary antibodies (goat anti-rabbit, Alexa fluor 488 and goat anti-mouse Alexa fluor 546, diluted in blocking buffer at 1:300) for 4 days at room temperature. The stained brains were washed in PBSD for 3x 45 min and RapiClear 1.52 (Sun Jin Lab) was used for tissue clearance lasting for 3h. Finally, the brains were permanently mounted in an iSpacer (0.55 mm, Sun Jin Lab).

Glomerulus segmentation

The z-stack scanning was implemented using a 20x objective (Objective W Plan-Apochromat 20x/1.0 DIC M27) with an Argon laser (488nm) and Helium-Neon laser (543nm) applying layer-adjusted laser power ranging from 15%-50% (ZEISS LSM 880). Scanning of a single focal plane was done at the recommended highest resolution with a duration of about 2 min to achieve high scanning quality. The used plane interval was 2 μm. For the purpose of glomeruli reconstructions, the z-stack scanning was terminated at the level of the globular lobe neuropil (i.e. projections from the palps) comprising approximately 120-130 planes. We used the Fiji plugin (segmentation editor) for glomeruli delineation and labeling and the segmentation software Amira (Thermo Fisher Scientific) for 3D visualization. To distinguish and identify single glomeruli, the Orco-positive and Orco-negative glomeruli were separately reconstructed using both, GFP and Synapsin fluorescent labeling. Two experimenters independently reconstructed the same specimen, resulting in a variation in the total number of glomeruli of less than 10%. We eventually reconstructed 3 antennal lobes of three locusts showing a high degree of stereotypy in terms of the total number and the proportion of Orco-positive glomeruli.

Two-photon calcium imaging

Locust dissection

Female locust nymphs at 2 days post-eclosion as well as immature adult females with the age of 3-5 days were used in our experiments. The locusts were starved for 2 h before the imaging experiments. Locust nymphs at stage 1-2 were immobilized in a customized plastic holder with a slit in the middle to fit the locust's cervical segment. Locusts at stage 3-6 were restrained with a cotton string to limit excessive movement and fixed in an upright tube with odorless clay. The locust's head was held up using a sterilized tooth stick to provide better access to the antennal lobe during the imaging experiment. The positioning of the cervical segment in the dissection tube was marked to mitigate variations resulting from embedding step. To facilitate the odor delivery, the locust's antenna was stretched horizontally by fixing the scape with clay. The locust's head capsule was opened using a sharp-pointed stab knife (22.5 degree), and excess tissue and trachea were carefully removed to ensure full access to the locust antennal lobe. During dissection, the locust saline buffer was constantly changed approximately 2 times per minute. To minimize brain movement during the experiment, the esophagus was pulled out of the body, and the brain was secured using a customized platform. To prevent any input from the ganglion, the two central nerve bundles were cut. The dissection process typically took 30-40 min, and the subsequent experiment lasted for 2-2.5 h. Animals beyond this duration were not used in further experiments to avoid potential declines in the physiological state of sensory neurons caused by excessive odor exposure.

Imaging setup

The dissected locust, secured in an upright tube, was attached to a plastic plate through a central hole that matched the operating platform of a 2-photon laser scanning microscope (2PCLSM, Zeiss LSM 710 meta NLO). The microscope was equipped with an

Please cite this article in press as: Jiang et al., Ring-shaped odor coding in the antennal lobe of migratory locusts, Cell (2024), https://doi.org/10.1016/j.cell.2024.05.036

infrared Chameleon UltraTM diode-pumped laser (Coherent, Santa Clara, CA, USA) and a 40x water immersion objective lens (W Plan-Apochromat 40x/1.0 DIC M27). Both the microscope and the laser were mounted on a smart table UT2 (New Corporation, Irvine, CA, USA). The fluorophore of GCaMP6s was excited using a wavelength of 925 nm.

Odor delivery

We used a computer-controlled odor delivery system as described before.[103] All the examined monomolecular odors were diluted in mineral oil (Figures 2, 3, 5 and S2–S4). 10 ml of the diluted odor was added to a 50 ml glass bottle (Duran Group, Mainz, Germany) equipped with two sealed openings for the in-and-out of the air flow. A continuous airstream at the speed of 1L/min controlled by a flowmeter was guided through a peek tube to the distal-middle part of locust's antenna. LabVIEW software (National Instruments) linked to the ZEN software (Zeiss) was implemented to control both image acquisition and odor delivery. Upon onset of odor delivery, the originally blocked valve was switched on temporarily to allow an airflow passing through the odor bottle and travelling to the locust's antenna. Odor application started 2 s after the onset of the recording and lasted for 2 s (i.e. frames 8-16, frame rate 4Hz) with a 2 min clean air interval between each odor application.

Odor name abbreviations: 25DP, 2,5-dimethyl-pyrazine; 4VA, 4-vinylanisole; APH, acetophenone; ANI, anisole; BAT, butyl acetate; BAL, benzyl alcohol; BPO, 1-butoxy-2-propanol; BZD, benzaldehyde; DAL, diacetone alcohol; DCE, decane; DEC, decanal; DEET, N,N-diethyl-meta-toluamide; DIH, dihydroactinidiolide; DIM, 1,3-dimethyluracil; DTP, 2,4,dimethoxyphenol; EOC, (E)-2-octen-1-ol; EHE, (E)-2-hexen-1-ol; EAT, 2-ethylhexyl acetate; ETH, ethyl hexanoate; GAC, geranyl acetone; GCA, γ-caprolactone; GES, geosmin; GUA, guaiacol; HAL, (E)-2-hexenal; HEP, 2-heptanone; HAC, hexanoic acid; IND, indole; IPH, isophorone; LAC, linoleic acid; LAT, L-alpha-terpineol; LIM, limonene; LIN, (+/−)-linalool; LOX, linalool oxide; MIS, 2-methyl-5-isopropylpyrazine; MBC, 2-methylbutyric acid; MOT, methyl oleate; OAL, octanal; OOL, 1-octen-3-ol, PAN, phenylacetonitrile; PEN, 1-pentanol; POX, α-pinene oxide; PAL, phenethyl alcohol; PAD, phenylacetaldehyde; SQL, squalene; TRI, 2,4,6-trimethylpyridine; VRT, veratrole.

Imaging procedure and data acquisition

The locust antennal lobe was centrally positioned to fit within the squared acquisition window (425 x 425 μm, for adult stage), and imaging experiments were performed from the dorsal side. We found a conserved glomerular organization at certain depths, which reoccurred in all animals. The first imaged plane was positioned approximately 20 μm below the dorsal surface of the antennal lobe, which usually contained an incomplete eyeball-shaped glomerular region. In the fourth plane (i.e. 60-70 μm), a complete view of the eyeball-shaped glomerular region appeared, while in the 10th focal plane Orco-negative glomeruli became visible. We estimate that these 10 focal planes cover 60%-70% of the total glomerular population. We used these features to evaluate each specimen before using it for the imaging experiment. We selected the odors PAN (10^{-3}) and linalool oxide (10^{-3}) as diagnostic odors to quantify the overall response strength of the specimen.

To resolve the chemotopic organization of locust antennal lobe at the adult stage (Figures 3, S3, and S4), 10 focal planes were imaged along the z-axis with an interval of 15 μm, corresponding to the mean size of a single glomerulus (Figure S1E). Prior to odor application, the imaged focal plane was scanned at high resolution (1024 x 1024 pixels) with appropriate laser power used for registration and glomerular identification. Each individual measurement consisted of a series of 40 frames (10 s duration) acquired at a resolution of 512 x 512 pixels at a frame rate of 4 Hz. For the imaging experiments of the 6 different developmental stages (Figure 5), we recorded odor responses in a single focal plane from each stage to 13 odors (concentration 10^{-3}), imaging 3-4 planes for each antennal lobe using the 40x water immersion objective. Due to the growing size of the locust antennal lobe, the z-axis interval between two imaged planes differed for the stages with 15 μm for stage 1 and 2, 20 μm for stage 3 and 4, 25 μm for stage 5 and 6. This configuration ensured that image acquisition was performed within a similar z-axis region of the locust antennal lobe across all stages. During image acquisition, the display of the locust antennal lobe for different stages was adjusted to fit a square acquisition window, allowing the projection of multiple focal planes from different stages (Figure 7).

Image data processing, analyses and presentation

ROI selection and validation

We used Fiji 2 for to process and present the imaging data. The acquired imaging data were first corrected for photobleaching using an exponential fit method. The data were then corrected for movement applying Fiji's StackReg plugin, using a high-resolution pre-experiment plane scan as a template. Based on the corrected imaging data, we calculated the F-F0 for the 40-frame imaging stacks, where F0 represented the averaged fluorescence of frames 1-6 (i.e. before odor application). To identify responsive ROIs, we obtained the averaged fluorescence values of frames 16-30, since this frame range captured the peak response for distinct OSN response modes.[57] Detailed Fiji settings include a FFT bandpass filter with a target object size setting as 10-100 pixels, a range covering the actual glomerulus size (Figure S1E), and with a tolerance of direction of 5%. The responsive ROIs were manually selected based on the filtered image with the help of PCA analysis of the dF image stacks, which highlighted the pixels that underwent large variations in fluorescence changes during the experiment. The boundary of each emergent ROI was delineated and its response traces were further quantified to determine the response amplitude. Basically, we used three criteria to select responsive ROIs: First, the peak raw amplitude (dF) of the selected ROI should be greater than 200 a.u. (i.e. fluorescence intensity), anything less was considered as noise. Second, the peak raw amplitude (dF) should exceed 3 times of the standard variation of frames 1-6. Third, the peak response (dF/F0) should exceed 20%. The response traces were also inspected to discard those with unusually large fluctuations. The actual locations of the validated responsive ROIs were slightly modified based on high resolution focal plane scans. Selection and validation of inhibitory responsive ROIs followed a similar methodology except that all criteria were inversed to negative values.

Please cite this article in press as: Jiang et al., Ring-shaped odor coding in the antennal lobe of migratory locusts, Cell (2024), https://doi.org/10.1016/j.cell.2024.05.036

Response map presentation

In this study, the response map merged onto one focal plane was presented in two forms: an unextracted and an extracted response map. The unextracted response map was constructed based on the averaged projection of frames 16-30, which was filtered and color-coded (dF, Figure S2). The extracted response map was constructed by extracting the responsive population from the projection of frames 16-30, which was then superimposed with the scanning of antennal lobe focal plane (dF, Figure 4; dF/F0, Figures 2 and S2).

Concentric ring region division

Inspired by the observation that odor-induced response patterns on a focal plane resemble a distinct ring-shaped structure, we sought to divide the glomerular region into even-width concentric ring regions. For simplicity, the centroid and the radius of the glomerular region on a focal plane were determined by fitting the outer boundary of the glomerular population into a circle. A distinct region was divided only based on its distance to the centroid relative to the diameter (relative distance, %), and was independent of any adjustment of raw imaging materials such as data rotation or alignment. The central hub region and its boundary, containing very few glomeruli, was divided into the most inner region (region 1), occupying a region spanning less than 25% of the width of the entire glomerular region. The remaining antennal lobe was divided into 15 concentric regions, each spanning 5% of the width of glomerular region. Each ring region and its corresponding spanning dimension (relative distance to the centroid, %) are listed below:

Ring-region	1	2	3	4	5	6	7	8	9	10	11	12	13	14	15	16
Dimension	<25%	25-30%	30-35%	35-40%	40-45%	45-50%	50-55%	55-60%	60-65%	65-70%	70-75%	75-80%	80-85%	85-90%	90-95%	95-100%

At the adult stage, the 5% of the glomerular region was estimated to be approximately 9-11 μm, slightly smaller than the minimum size of s single glomerulus (Figure S1E), thus providing a fine resolution of rendering the regional response weights. For a very few glomeruli whose actual locations were estimated to be greater than 100% of the diameter, they were treated as belonging to the most peripheral region (region 16). The 16-region paradigm was applied to nymphal locusts, whose antennal lobe was smaller than that of adults (Figure 5F).

Regional response weights

The large number of glomeruli comprised within the locust antennal lobe does not allow to identify each individual glomerulus. Instead, to examine the chemotopic organization in the locust antennal lobe, we introduced an approach that integrates both the population size and the response strength of the responsive glomerular population in a defined concentric ring-shaped region. To examine the chemotopic organization induced by monomolecular odors (Figure 3) or headspaces (Figure 4), we pooled the responses of the glomerular population deriving from all focal planes from all the tested animals. The response weight in a region k: $\bar{r}p(k)$ was determined as:

$$\bar{r}p(k) = (\bar{r}_k * p_k) \Big/ \sum_{k=1}^{16} (\bar{r}_k * p_k)$$

where $\bar{r}_k$ represents the mean peak response (dF/F0) of the glomerular population distributed in the region k, while p_k denotes the percentage of the size of responsive glomeruli in the region k relative to that of the entire responsive population identified in the antennal lobe (%). To compare the regional response profile among tested odors, the response weights in a specific region was z-score normalized among odors. The matrix of normalized regional response weights was analyzed in a hierarchical clustering using the Ward group method with the calculated Manhattan distance matrix (Figure 3).

Glomerular response space and cluster identification

To investigate the intrinsic coding properties of the glomerular clusters, we exposed animals from the 6 developmental stages to a panel of 13 odors in each focal plane. A glomerulus was considered responsive if it showed a valid excitatory response (criteria see above) to at least one of the 13 odors, while those showing only inhibitory responses were excluded from the analysis. This yielded an identification of over 11000 responsive glomeruli. The response profile of each glomerulus to the 13 tested odors was normalized to the maximum response (set at 100%), while the responses below 20% were treated as 0. To visualize the landscape of glomerular population coding in a 2D space, we used the tSNE algorithm with specific parameters (perplexity 200, exaggeration 1, PCA components 5) to process the normalized dataset. We used the Louvain algorithm for glomerular cluster identification, a method for community detection in large networks, using the cosine distance matrix based on the normalized data set. This clustering algorithm allows for a flexible clustering membership by adjusting the resolution, a parameter responsible for the deduced cluster size or number.[77–79] Since the size of a functional glomerular cluster was unknown, we first determined the minimum cluster size (i.e. the number of nearest neighbors to use to form the KNN graph) by assuming that the cluster members should appear in at least half of the total tested layers, i.e., 0.5 * 139. To approximate the number of glomerular clusters derived from a panel of 13 tested odors, we adjusted the clustering resolutions at 1, 0.5, 0.3, 0.2, and 0.1, respectively. The default resolution implemented in Louvain clustering is 1 and the maximum resolution is 0.1. The five adjusted resolutions result in the deduced cluster numbers of 27, 37, 47, 54 and 71, respectively. The "animal occurrence rate" is considered as an important parameter to justify the presence of clusters: the

Please cite this article in press as: Jiang et al., Ring-shaped odor coding in the antennal lobe of migratory locusts, Cell (2024), https://doi.org/10.1016/j.cell.2024.05.036

detection of one cluster (i.e., the glomerulus members) in many replicates makes the existence of this cluster more likely. We consider that a common glomerular cluster should be present at least in more than 80% of the tested animals at a given stage, corresponding to 6 out of the 7 tested animals.

Locust chemospace

A comprehensive set of chemical descriptors for 209 odors were used for constructing the locust chemospace. The odor array included the ecological relevant odor-base for *Locusta migratoria*[46] as well as a few other odors, such as DEET and geosmin. We used the software Dragon 5.0 to calculate chemical descriptors underlying the chemical's 2D chemometric features. Among the generated 2489 chemical descriptors, a large population of them were 0 for all the 209 odors, which were not considered for subsequent analysis. We eventually screened 799 non-0 chemical descriptors and each of the descriptors was z-score normalized among the 209 odors. We note that a much smaller set of weighted chemical descriptors was recommended for the chemical structure calculation.[104] Since many locust odors present in our analysis were not included in the previous study, in our study we used a larger set of descriptors. The normalized 799 descriptors were used for further chemospace construction and structure similarity determination. The multidimensionality of the 209 odors was reduced to a 2D virtual space using the tSNE algorithm (perplexity 100, exaggeration 1, PCA components 20) implemented in Orange 3.0. The structural correlation was determined by calculating the Pearson correlation of the set of 799 descriptors for each of the odor pairs.

Headspace analysis

Headspace collection

Five types of headspace were generated and used directly for the imaging experiment. Locusts were starved for 2 h to eliminate any residual food odors from their bodies. Plants were collected fresh from the growing soil without any additional treatment. To mimic the natural scenario, the headspace of adult locusts consisted of 13 pairs of males and females aged between 5-10 days. Similarly, the headspace of nymphs consisted of 30 5th instar locusts, with both males and females aged 2-4 days after eclosion. The locusts were crowded into a spacious container, consisting of four interconnected lock&lock boxes (approximately 5 liters of space, LocknLock company), and placed in a climate chamber at 30 °C for 4 hours. This setup has been shown to be effective in previous imaging experiments, and the animals were not harmed by hypoxia. For the plant-derived headspaces, 150 g of leaves were used, and the plants were of slightly different ages (maize, 5 weeks; wheat, 4 weeks; and rapeseed, 5 weeks). The plant leaves were cut into small pieces to mimic herbivore foraging and placed in the same container as the locusts but at room temperature for 4 hours. The lock&lock box container was equipped with two openings, similar to the odorant bottle described above, and was attached to our odor delivery system. The far dorsal region of the locust antennal lobe was disregarded, as it contained a sparse responsive population for all five headspace types. Therefore, only seven focal planes were imaged within a single antennal lobe with a z-axis spacing of 15 μm. The collected headspaces were used for a single trial, with each individual animal tested with only one antennal lobe side. This approach was adopted to account for any potential weaker responses that might occur due to decreasing headspace concentration.

GC-MS analysis of chemical identity

The volatile content of each of the five headspaces was identified using solid phase microextraction (SPME).[46] The customized lock&lock box used for the imaging experiments was also used for headspace collection. Locust-related headspaces were collected at 30°C for 20 h, while the plant-related headspaces were collected at room temperature for 20 h. Headspace from an empty lock&lock box was used as a control. After each headspace collection, the SPME fiber was retracted and immediately applied to the inlet of a gas chromatography–mass spectrometry (GC–MS) system equipped with an HP5 column. The GC-MS running program was set as follows: the column temperature was initially maintained at 40°C for 3 min and then increased to 150°C at 5°C·min^{-1}, then increased to 260°C at 10°C·min^{-1}, followed by a final step of 5 min at 260°C. Compounds were identified by comparing the obtained mass spectra against synthetic standards and NIST 2.0 library matches. The identity of each compound was validated by the R-match value (R>0.85) and the ambiguous volatiles were neglected for the analysis. The content of each compound was determined as the area under the peak and the minor compounds, which were less than 2% of the most abundant compound, were not considered. In general, only the top half of the abundant compounds was used for enrichment analysis. Compound content was further corrected by the blank control. The chemical distance for the identified abundant compounds was determined based on a set of non-0 chemical descriptors as reported in the *Locust Chemospace* session.

Predicting OR distribution

To predict the spatial distribution of locust ORs, we first extracted the response profile of locust OR types using a panel of 13 odors that were comprised in a recent study of functional deorphanization of locust ORs.[46] The panel of 13 odors represents a diverse set of chemical classes and is therefore sufficient to capture the response profile of locust ORs. We considered a total of 18 candidate OR types that showed responsiveness to at least one of the 13 odors with a strength of at least 50% of the maximum responsiveness elicited by the 13-odor panel. The extracted response profiles of the candidate OR types were analyzed with Louvain clustering along with the characterized glomerular population in former study (in total 11,884 glomeruli). In each independent clustering analysis, using the same dataset we gradually adjusted the clustering resolution parameter to 3, 2, 1, 0.5 and 0.2, respectively. A candidate OR type is grouped with a subset of the glomerular population. The five independent clustering analyses generate partially overlapping

Please cite this article in press as: Jiang et al., Ring-shaped odor coding in the antennal lobe of migratory locusts, Cell (2024), https://doi.org/10.1016/j.cell.2024.05.036

memberships, highlighting a basic group of glomeruli that occurs in most clustering operations. Therefore, this basic group is most closely related to the candidate OR type. The occurrence rate of the basic glomeruli grouped with the candidate OR type across the five independent clustering analyses was considered as the "likelihood", indicating the potential distribution of the candidate ORs in the antennal lobe.

Tracing and reconstruction of OSNs and PNs

To label individual OSNs, adult female locusts (Orco-Syn-GCaMP6) were fixed and immobilized in a glass slide with the scape embedded in clay to prevent movement. We used a sharp blazer to destroy the cuticle of the sensilla and antenna by gently scratching the dorsal surface of the antenna. Since OSNs are enriched in the distal to mid-antenna region, the scratching was limited to this area. Once the wound was created, the antenna was wrapped with a capillary containing 5% Neurobiotin (Vector Laboratories). The animal was kept overnight at room temperature in the dark. For intracellular PN staining, adult female locusts were briefly anaesthetized in 4°C and embedded in a custom-built plastic container with the head restrained using modeling clay or dental wax. A small window was opened frontally in the head cuticle and the antennal lobe was exposed after removing gland and fat sheaths. The head capsule hemolymph was replaced by locust saline buffer. Then the tip of a sharp borosilicate glass capillary (Hilgenberg GmbH, Malsfeld, Germany), pulled with a horizontal laser puller (P 2000, Sutter Instruments, Corp., Novato, CA, USA), and filled with MicroRuby (dextran, tetramethylrhodamine and biotin, 3000 MW), was inserted into the PN cell body layer located on the surface of the antennal lobe, operated by the use of a manual micromanipulator. The dye was injected iontophoretically by applying a depolarizing current (2-20 nA) for 10-30 min. with a bridge amplifier (BA-03X, npi electronic GmbH, Tamm, Germany). A silver wire immerged into the head capsule's saline buffer served as a reference electrode. After dye injection and incubation, locusts were kept in a humid chamber at 4°C overnight, after which the brains were dissected, fixed in 4% PFA for 2 h at room temperature, rinsed in PBS, dehydrated in ascending ethanol series and cleared in methyl salicylate for confocal microscopic scans. Reconstruction of OSN and PN morphology was done with the segmentation editor and the semi-automated skeleton tree module in Amira (Thermo Fisher Scientific).

QUANTIFICATION AND STATISTICAL ANALYSIS

Analyses of calcium imaging data were performed using Fiji 2. Correlations in this study were indicated by Pearson's *r* correlation with the significance at 0.05 level. For all statistical analyses, Origin 2023b was used, where the data distribution was examined with the Kolmogorov–Smirnov test for two-sample comparison and the group variance was examined with Levene's test for multiple comparisons. Two-tailed Student's t test was used in Figures S1 and S4. Multiple comparisons were performed with one-way ANOVA in Figure S5 and Kruskal-Wallis test in Figure S6. Statistical significance was set at 0.05 level. In box plots and line graphs, data were presented as mean ± SEM (Figures 4, 5, S1, and S3–S6). In box-and-whisker plots, the range of data is indicated in the figure legends (Figures S4 and S5). Sample size and animal replicates were clarified in the corresponding figure legends.

CellPress
OPEN ACCESS

Supplemental figures

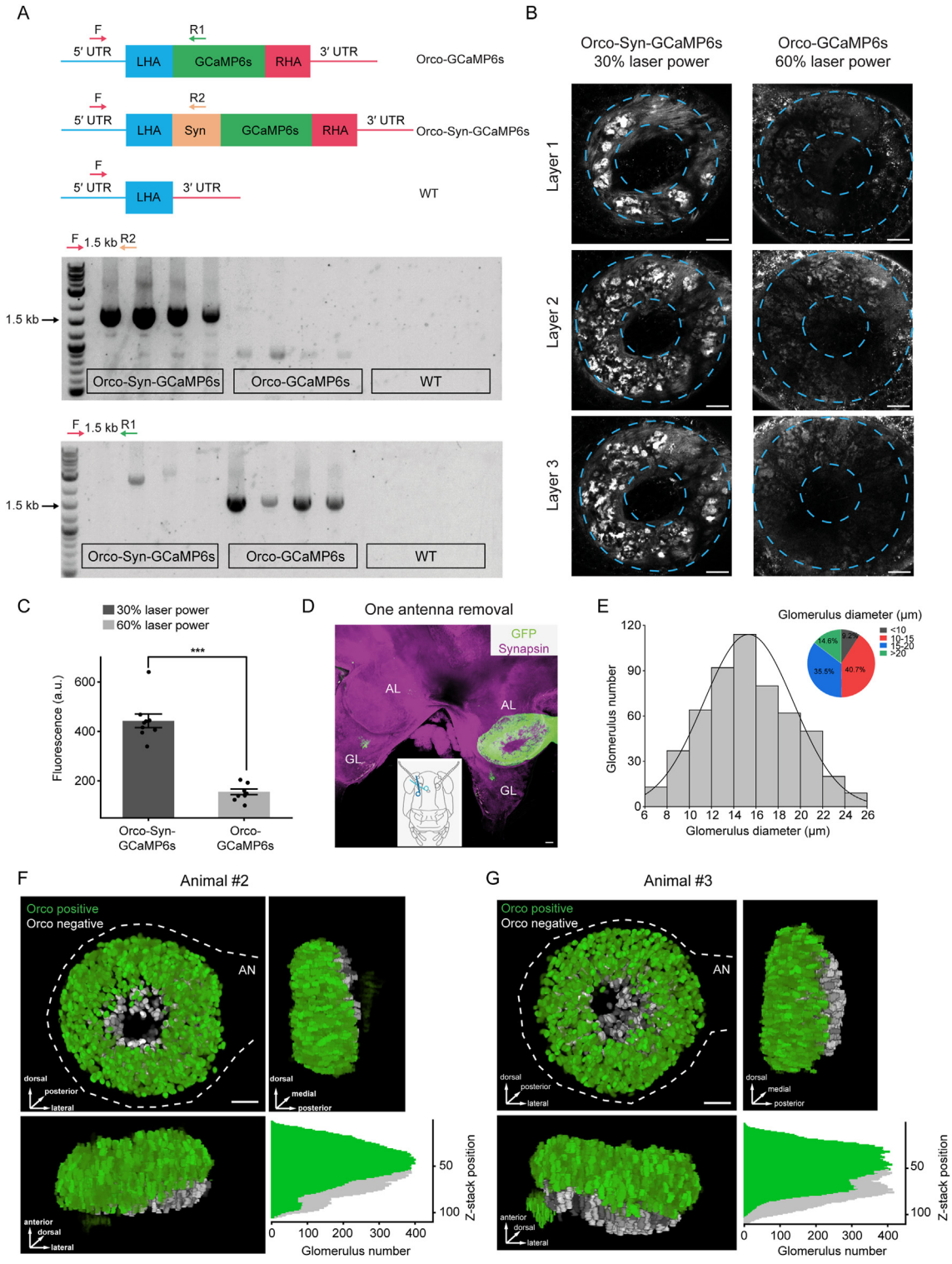

(legend on next page)

Figure S1. Genotyping, phenotypic quantification, and stereotypic antennal lobe organization, related to Figure 1

(A) Genotyping of two types of transgenic locusts. The consensus primer F is located on the 5′ UTR beyond the left homology arm (LHA, 1 kb), and the insertion-specific primers R1 and R2 are located on the 5′ region of GCaMP6s and synaptophysin (Syn), respectively. Both primer pairs F-R1 and F-R2 are supposed to generate an amplicon with the size of approximately 1.5 kb in corresponding genotypes. No amplicons are expected in the wild-type (WT) locusts using either primer pair.

(B) Scanning of three focal planes in the dorsal region of the locust antennal lobe from two genotypes. 30% and 60% laser power were used for *Orco-Syn-GCaMP6s* and *Orco-GCaMP6s* locusts, respectively. The interval between scanned planes is 10 μm. Scale bars, 50 μm.

(C) Lower laser power induced much stronger fluorescence intensity in *Orco-Syn-GCaMP6* locusts. Data are represented as mean ± SEM. Student's t test, $^{***}p < 0.001$. $n = 9$ focal planes from 3 animals.

(D) Ipsilateral OSN projection in the locust antennal lobe. GFP and synapsin were immunostained in *Orco-Syn-GCaMP6s* locusts at 10 days post removal of the antenna on the right side. No contralateral projections could be seen. OSN innervation from the palp to the globular lobe (GL) remains on both sides.

(E) Quantification of glomerular diameter visualized on a single focal plane. Glomeruli from the top three focal planes in Figure 1D were quantified.

(F and G) Conserved gross glomerular organization in the locust antennal lobe visualized with GFP immunostaining. Two independent specimens were visualized at three different perspectives like in Figure 1E. Lower right, number of glomeruli for each focal plane.

Scale bars, 50 μm.

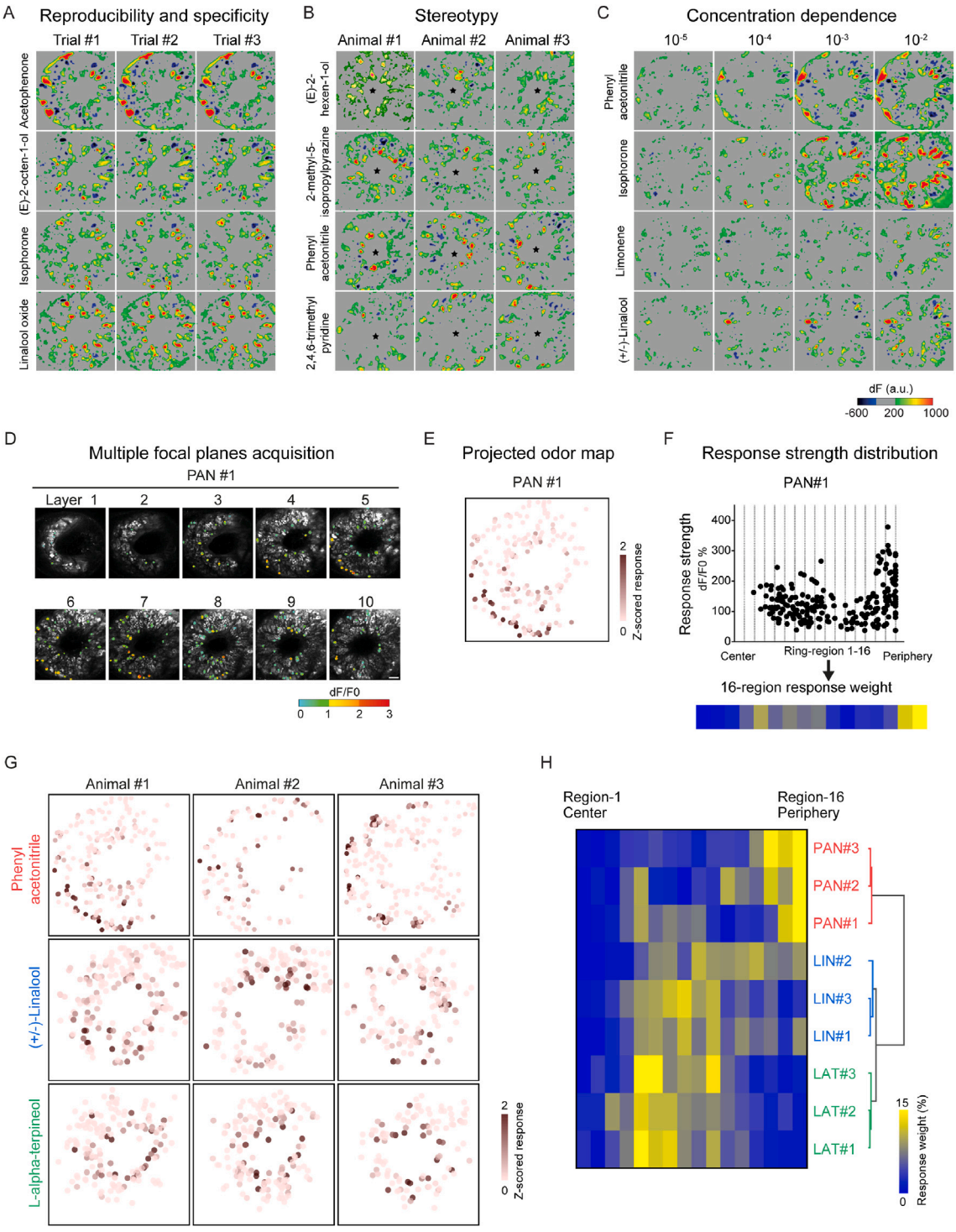

Figure S2. Odor maps for single focal plane and for multiple focal planes across the antennal lobe, related to Figures 2 and 3

(A) Odor-evoked fluorescent changes (dF) on a single focal plane for three consecutive trials, related to Figure 2A.

(B) Odor-evoked fluorescent changes (dF) on a single focal plane for three animals, related to Figure 2B. The centroid is marked as a black pentagon.

(C) Odor-evoked fluorescent changes (dF) on a single focal plane for increasing concentrations, related to Figure 2C.

(D) Example of response maps with 10 focal planes (animal #1) after antennal stimulation with PAN (10^{-3}). For clarity, only excited glomeruli were extracted and presented. Scale bars, 50 μm.

(E) Projected odor maps after antennal stimulation with PAN (10^{-3}) for animal #1.

(legend continued on next page)

(F) Regional distribution of responsive glomeruli and determination of the 16-region response weight. For each responsive glomerulus, its relative distance to the centroid is represented on the x axis, while its response strength is depicted on the y axis.
(G) Similar projected odor maps for three odors across three animals.
(H) A hierarchical clustering of the projected odor maps using their regional response weights. Odor abbreviation: PAN, phenylacetonitrile; LAT, L-alpha-terpineol; LIN, (+)-linalool.

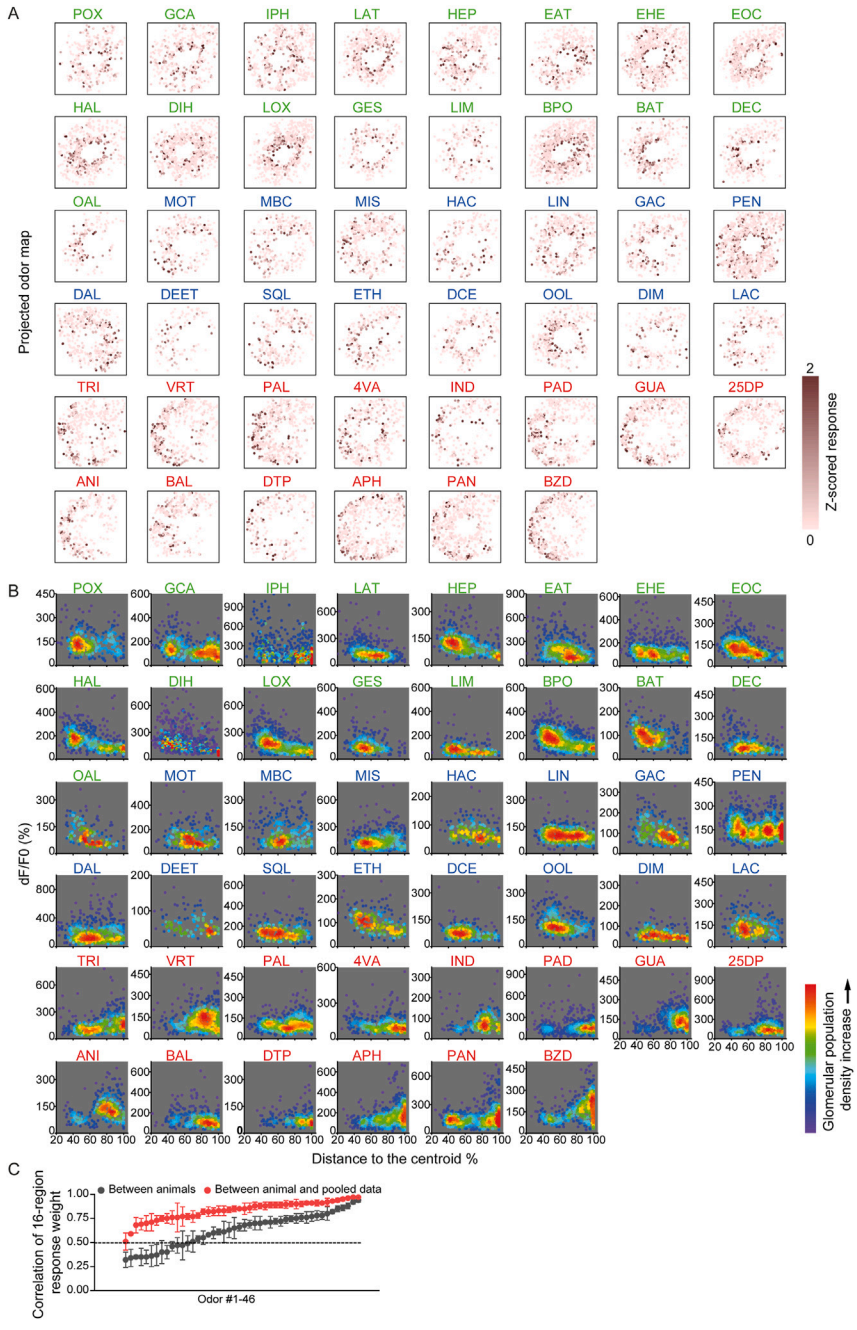

Figure S3. Projected odor maps and centroid-based distributions of glomerular responses for 46 odors, related to Figure 3

(A) Z-projected odor maps for the 46 tested odors.

(B) The centroid-oriented distribution of excitatory glomerular responses for the 46 tested odors (n = 3). The color code represents the density of the responsive glomerular population, with warm colors (i.e., red/ yellow) indicating densely clustered glomeruli, while sparsely distributed glomeruli are shown in cold colors (i.e., blue). Odor names were colored according to Figure 3D.

(C) Correlation analysis of the 16-region response weight between the three tested animals (black data points) and between each animal and the pooled data (red data points). A strong correlation (r = 0.5) across individuals is indicated by a dashed line. The pooled data were collected from three animals. Data were presented as mean ± SEM.

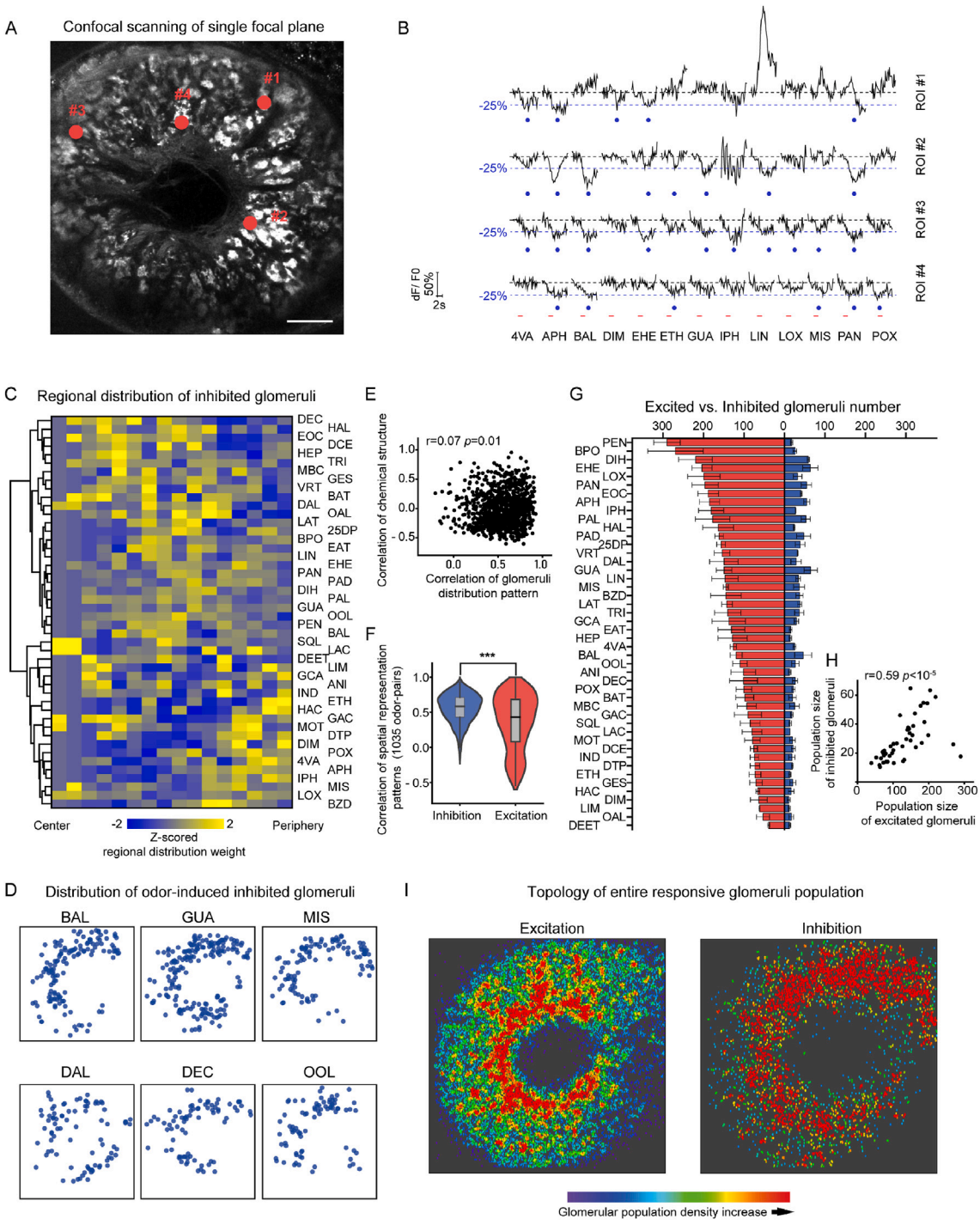

Figure S4. Spatial distribution of inhibited glomeruli is less odor specific, related to Figure 3

(A) Confocal scanning of a single focal plane with four glomeruli indicated, where responses were measured (#1–#4). Scale bar, 50 μm.

(B) Dynamic odor response traces for the four distinct glomeruli indicated in (A). Red line indicates the stimulus duration (2 s). Odor-induced inhibitory responses are marked with blue dots. A response with a peak lower than −25% of dF/F0 was categorized as an inhibitory response.

(C) Hierarchical clustering of the regional distribution of inhibited glomeruli for 46 tested odors. For odor abbreviations please see figure legends of Figure 3.

(D) Spatial distribution of inhibited glomeruli for six odors. n = 3 female adults for each odor.

(E) Correlation of the distribution of inhibited glomeruli and chemical structure. n = 1,035 odor pairs from 46 odors. r, Pearson correlation.

(F) Inhibited glomeruli exhibit more homogeneous spatial representation patterns than excited glomeruli. n = 1,035 odor pairs from 46 odors. Box-and-whisker chart, median within data range of 25%–75% and the 1.5 inter-quartile range. ***$p < 0.001$, paired Wilcoxon signed-rank test.

(legend continued on next page)

(G) The number of excited and inhibited glomeruli after antennal stimulation with 46 different odors. Data are represented as mean ± SEM. *n* = 3 animals for each odor.
(H) Correlation of the number of excited and inhibited glomeruli for each odor stimulation. r, Pearson correlation.
(I) Topology of accumulated excited (left) and inhibited (right) glomeruli. Density plot integrates a projection of the entire activated glomerular population after antennal stimulation with the 46 odors tested.

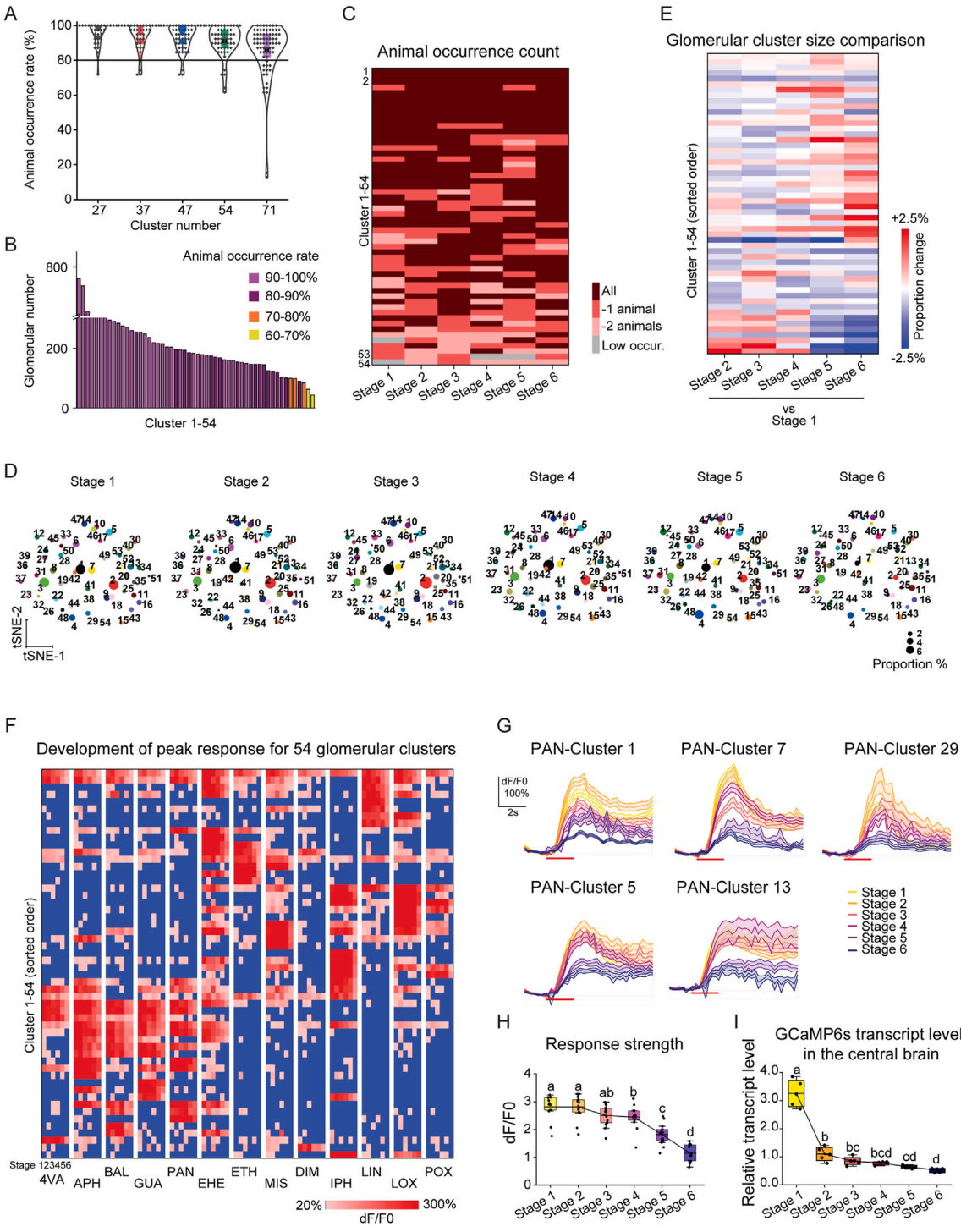

Figure S5. Clustering validation and the development of response strength and glomerular cluster size, related to Figure 6

(A) Occurrence of the deduced cluster numbers resulting from the clustering analyses in the 39 animals tested. Each of the deduced cluster number is derived from independent clustering analysis using the same dataset with adjusted resolution parameter in the implemented Louvain clustering algorithm. See STAR Methods for details. Box and distribution plots represent the mean and data range of 10%–90%.

(B) Number of glomeruli in each cluster. The majority of the clusters show an animal occurrence rate of over 80% with only a small number falling below 70%.

(C) Animal occurrence count for each of the 54 clusters at six developmental stages. Each stage comprises 6–7 animals.

(D) Simplified glomerular response space across the six developmental stages. Each cluster was simplified as a dot representing the centroid of cluster members with the dot size proportional to the relative cluster size.

(legend continued on next page)

(E) Development of glomerular cluster sizes. The relative population size of each glomerular cluster for stage 2–6 was compared with the initial stage 1.
(F) Development of peak responses of the 54 clusters. Individual columns contain 54 blocks showcasing the mean response of cluster members at each of the 6 stages to a given odor. Clusters not responding to a given odor (below 20% of dF/F0) are denoted in blue.
(G) Raw response traces of five representative clusters to PAN (10^{-3}). The bold line and shaded area represent mean ± SEM.
(H) A gradual decrease of general response strength through development. Data points represent the averaged glomerular response strength for each of the 13 tested odors. Box-and-whisker chart represents mean ± SEM within data range of 25%–75%. One-way ANOVA with Fisher's least significant difference (LSD) post hoc test.
(I) Transcript level of GCaMP6s in the locust brain throughout developmental stages. *n* = 4–5 replicates. Box-and-whisker chart represents mean ± SEM within data range of 25%–75%. One-way ANOVA with Fisher's LSD post hoc test.

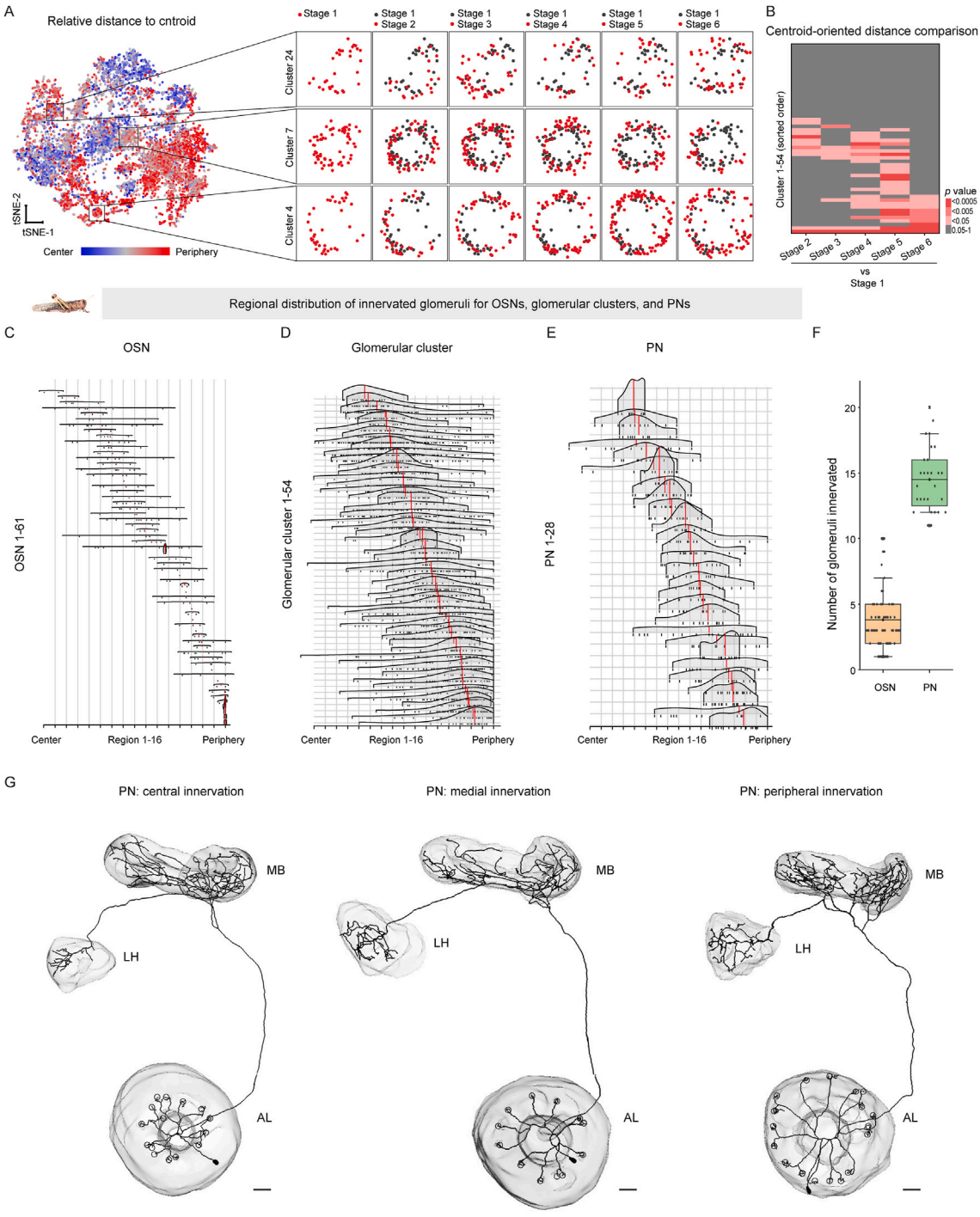

Figure S6. The ring-shaped glomerular organization is preserved across stages and is a shared characteristic with PN dendritic arborizations, related to Figure 7

(A) Visualization of the ring-shaped organization of glomerular clusters across different stages. Left, plot of the relative distance to the centroid in the glomerular response space. Right, examples of three glomerular clusters representative for glomerular innervations in the medial, central, and peripheral antennal lobe regions, respectively.

(B) Comparison of the relative distance to the centroid exhibited by glomerular clusters across stages. *p* values for differences between stages 2–6 and stage 1 are color coded. The gray color indicates the statistically insignificance regarding the distance comparison for a specific glomerular cluster between two stages. Relative distance comparison: Kruskal-Wallis ANOVA, Dunn's post hoc test, *p*, significance at 0.05 level.

(legend continued on next page)

(C–E) Ridgeline plots of the spatial distribution of OSN axonal innervation, glomerular clusters, and PN dendritic innervation. The glomerular population innervated by a single type of OSN (C), glomerular cluster (D), or PN (E) is represented as rugs on the x axis within the 16 concentric ring regions. Individual backfills or clusters are displayed on the y axis. The median location of the innervated glomerular population by a single backfill or cluster is indicated by a red line. The distribution is represented as a kernel density plot, with the height of the curves scaled to their respective maximum values.
(F) The number of glomeruli innervated by single OSNs and PNs. Box-and-whisker plot represents mean within a data range of 10%–90%.
(G) Complete morphologies of three PNs representing glomerular innervation in the central, medial, and peripheral antennal lobe regions, respectively. Scale bars, 50 μm.

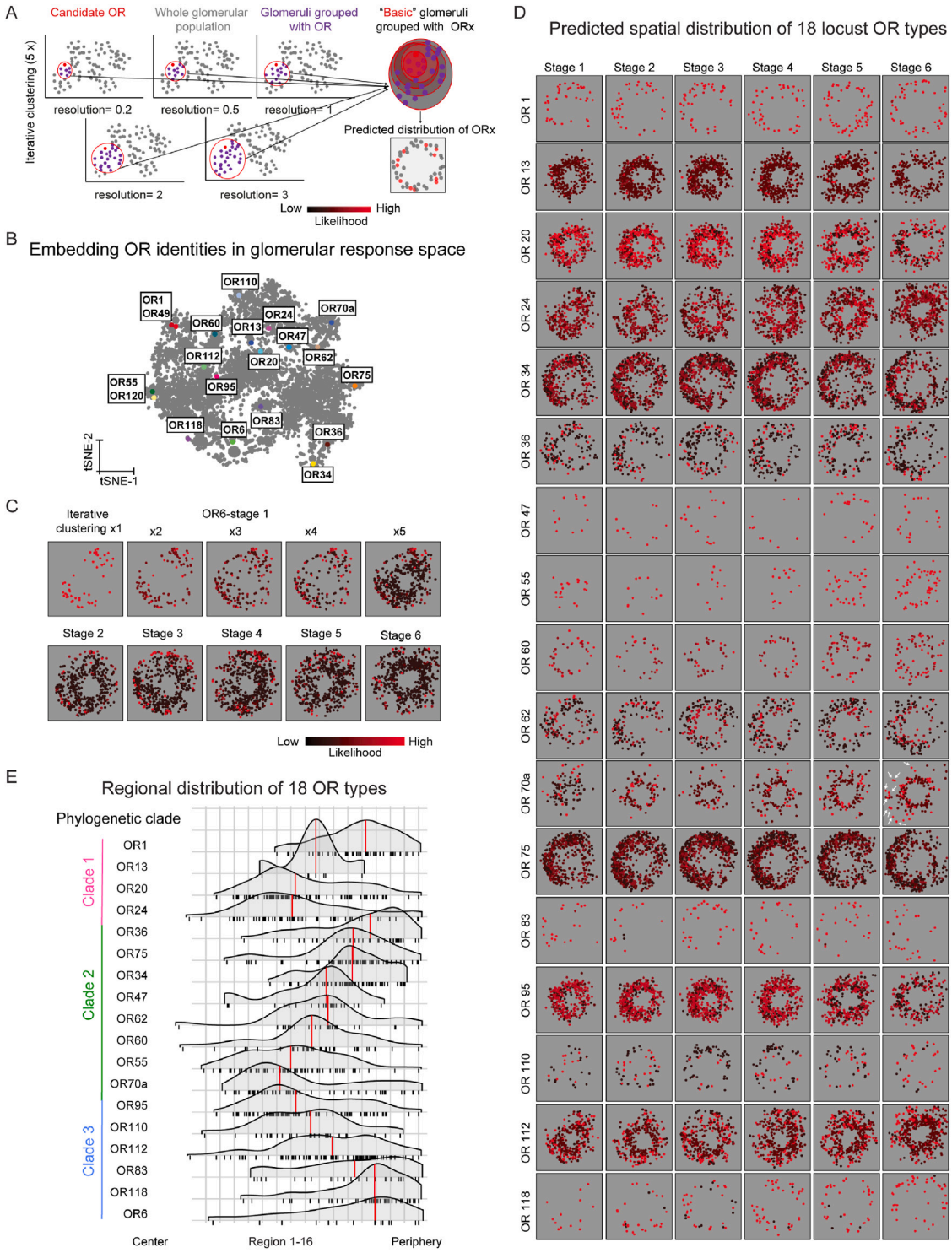

Figure S7. Predicted spatial distribution of specific OR types in the locust antennal lobe, related to Figure 7

(A) Workflow for predicting the spatial distribution of glomeruli associated with distinct OR types in the locust antennal lobe. The five independent clustering analyses generate partially overlapping cluster memberships, and the basic glomeruli grouped with the candidate OR type across multiple clustering operations are more related to the OR type. For details, please see STAR Methods.

(B) Embedding OR identities in the glomerular response space. ORs with identical extracted response spectra are together in a box.

(C) Proposed spatial distributions of OR6 at stage 1 (upper) and at stages 2–6 (lower) via iterative clustering analyses. A higher likelihood indicates that a glomerulus was more frequently grouped together with the candidate OR type.

(legend continued on next page)

(D) Prediction of the spatial distribution of glomeruli associated with each of the 18 OR types across the 6 developmental stages. Generation of the likelihood-indicated spatial distribution map was based on the deduced membership from the iterative clustering analyses (5×) by progressively adjusting the resolution. See STAR Methods for details. The predicted distribution of OR70a glomeruli at adult stage that is located in the peripheral antennal lobe region is highlighted by white arrows.

(E) Ridgeline plot of predicted regional distributions of glomeruli associated with each of the 18 OR types in the locust antennal lobe. The plotted glomeruli comprise the basic glomeruli that were more frequently grouped with a candidate OR type in the iterative clustering analyses (likelihood $\geq$ 0.8). The median location of innervated glomeruli is indicated by a red line. The distribution is represented as a kernel density plot, with the height of the curves scaled to their respective maximum values. Classification of the phylogenetic clades and the included OR types derived from Wang et al.[45]